© 2020. Published by The Company of Biologists Ltd | Development (2020) 147, dev193417. doi:10.1242/dev.193417

STEM CELLS AND REGENERATION

RESEARCH ARTICLE

β-Catenin drives distinct transcriptional networks in proliferative and nonproliferative cardiomyocytes

Gregory A. Quaife-Ryan[1,2], Richard J. Mills[1], George Lavers[1], Holly K. Voges[3], Celine J. Vivien[3], David A. Elliott[3,4,5], Mirana Ramialison[4], James E. Hudson[1,*] and Enzo R. Porrello[3,6,*]

ABSTRACT

The inability of the adult mammalian heart to regenerate represents a fundamental barrier in heart failure management. By contrast, the neonatal heart retains a transient regenerative capacity, but the underlying mechanisms for the developmental loss of cardiac regenerative capacity in mammals are not fully understood. Wnt/β-catenin signalling has been proposed as a key cardioregenerative pathway driving cardiomyocyte proliferation. Here, we show that Wnt/β-catenin signalling potentiates neonatal mouse cardiomyocyte proliferation *in vivo* and immature human pluripotent stem cell-derived cardiomyocyte (hPSC-CM) proliferation *in vitro*. By contrast, Wnt/β-catenin signalling in adult mice is cardioprotective but fails to induce cardiomyocyte proliferation. Transcriptional profiling and chromatin immunoprecipitation sequencing of neonatal mouse and hPSC-CMs revealed a core Wnt/β-catenin-dependent transcriptional network governing cardiomyocyte proliferation. By contrast, β-catenin failed to re-engage this neonatal proliferative gene network in the adult heart despite partial transcriptional re-activation of a neonatal glycolytic gene programme. These findings suggest that β-catenin might be repurposed from regenerative to protective functions in the adult heart in a developmental process dependent on the metabolic status of cardiomyocytes.

KEY WORDS: Cardiac regeneration, Cardiomyocyte proliferation, Metabolism, Transcriptional regulation, Wnt/β-catenin

INTRODUCTION

For >30 years it has been recognised that cardiomyocyte proliferation is shut down during early postnatal development of the mammalian heart (Rumyantsev and Borisov, 1987; Soonpaa et al., 1996). As proliferative potential is lost, cardiomyocytes undergo maturation, whereby fetal/neonatal genes encoding structural, cell cycle and metabolic proteins are exchanged for mature adult transcriptional programmes to meet the functional demands of postnatal life (Taegtmeyer et al., 2010). Hence, the global transition from an immature to a mature state involves changes in almost every facet of cardiomyocyte physiology, including loss of cardiomyocyte proliferative potential. However, the molecular processes that govern the transitions from hyperplastic to hypertrophic growth remain poorly characterised. After myocardial infarction (MI) in adult mammals (where ∼25% of cardiomyocytes perish), the very low basal rate of adult cardiomyocyte turnover (<1%) is insufficient to restore damaged cardiomyocytes and recover heart function (Bergmann et al., 2015). By contrast, during the first days of life, when cardiomyocytes are actively proliferating, neonatal mammals possess a robust, albeit transient capacity for cardiac regeneration (Porrello et al., 2011; Ye et al., 2018; Zhu et al., 2018). Therefore, understanding and modulating the processes by which cardiomyocytes mature and cease proliferating in the postnatal window could lead to potential therapies for heart failure patients.

A host of postnatally regulated factors have been linked to the loss of cardiomyocyte proliferative capacity, including cyclins and cyclin-dependent kinases (Mohamed et al., 2018), tumour suppressors (Sdek et al., 2011), transcription factors (Heallen et al., 2011; Mahmoud et al., 2013), microRNAs (Eulalio et al., 2012; Porrello et al., 2013), growth factor receptors (D'Uva et al., 2015), hormones (Hirose et al., 2019), vagal innervation (Mahmoud et al., 2015), metabolic substrates (Mills et al., 2017), immune factors (Aurora et al., 2014; Natarajan et al., 2018), extracellular matrix components (Bassat et al., 2017), epigenetic programming (Quaife-Ryan et al., 2017) and the oxidative postnatal environment (Nakada et al., 2017). Although modulation of these processes stimulates cardiomyocyte proliferation, none completely regenerates the adult heart after MI.

We previously undertook an extensive multicellular transcriptional analysis of the neonatal and adult mouse heart to identify drivers of cardiac regeneration and uncovered a possible role for Wnt/β-catenin signalling (Quaife-Ryan et al., 2017). We subsequently screened pro-proliferative factors in human pluripotent stem cell (hPSC)-derived cardiac organoids (hCOs) *in vitro* and discovered that β-catenin signalling was repressed during cardiac maturation (Mills et al., 2017). Although the contribution of Wnt/β-catenin to neoplastic diseases is well characterised, confusion exists surrounding the exact role of β-catenin in the postnatal heart. Contradictory evidence suggests that β-catenin drives adult cardiomyocyte hypertrophy (Chen et al., 2006; Hahn et al., 2006) or adult cardiomyocyte hyperplasia (Iyer et al., 2018) and can be cardioprotective (Hahn et al., 2006) or facilitate pathological cardiac remodelling (Iyer et al., 2018). Moreover, cardiac regenerative pathways, such as Hippo/Yap, insulin-like growth factor, peroxisome proliferator-activated receptor delta and neuregulin/Erbb2, co-opt β-catenin signalling to stimulate cardiomyocyte proliferation (D'Uva et al., 2015; Heallen et al., 2011; Magadum et al., 2017; Xin et al., 2011). Likewise, Wnt/β-catenin signalling induces immature hPSC-derived cardiomyocytes

[1]QIMR Berghofer Medical Research Institute, Herston, Brisbane, Queensland 4006, Australia. [2]School of Biomedical Sciences, The University of Queensland, St Lucia, Brisbane, Queensland 4072, Australia. [3]Murdoch Children's Research Institute, The Royal Children's Hospital, Parkville, Victoria 3052, Australia. [4]Australian Regenerative Medicine Institute, Monash University, Clayton, Victoria 3800, Australia. [5]Department of Paediatrics, The Royal Children's Hospital, University of Melbourne, Parkville, Victoria 3052, Australia. [6]Department of Physiology, School of Biomedical Sciences, The University of Melbourne, Parkville, Victoria 3010, Australia.

*Authors for correspondence (enzo.porrello@mcri.edu.au; james.hudson@qimrberghofer.edu.au)

M.R., 0000-0001-6315-4777; J.E.H., 0000-0003-0832-9356; E.R.P., 0000-0001-6105-7463

Handling Editor: Benoit Bruneau
Received 1 June 2020; Accepted 18 October 2020

Development (2020) 147, dev193417. doi:10.1242/dev.193417

(hPSC-CMs) and neonatal human atrial cardiomyocytes to proliferate *in vitro* (Mills et al., 2017; Wang et al., 2016), whereas other studies suggest that β-catenin is activated only in cardiomyocytes of human failing hearts (Hou et al., 2016). Wnt/β-catenin signalling is activated in several cell types post-infarction (cardiomyocytes, endothelial cells, leukocytes, Sca-1^{+}/c-Kit^{+} progenitor cells and fibroblasts) (Oerlemans et al., 2010). However, the cell type-specific functions of Wnt/β-catenin signalling in these diverse cardiac cell populations have not been fully elucidated. Hence, Wnt/β-catenin function appears to be highly context dependent, and its role in cardiomyocyte proliferation and maturation remains poorly delineated.

Here, we demonstrate that β-catenin augments proliferation of immature neonatal mouse cardiomyocytes and immature hPSC-CMs. By contrast, β-catenin deploys a cardioprotective response in the adult heart that is independent of cardiomyocyte proliferation. The adult cardioprotective response is associated with partial transcriptional reversion towards an immature cardiomyocyte metabolic state. This study also shows that β-catenin drives distinct transcriptional programmes associated with proliferative networks in regenerative cardiomyocytes and immunomodulatory networks in nonregenerative adult cardiomyocytes. Hence, β-catenin stimulates immature cardiomyocyte proliferation but is unable to drive adult cardiac regeneration. Finally, it is proposed that pro-proliferative factors, such as β-catenin, might be repurposed from proliferative to protective functions in the adult heart in a process dependent on the metabolic status of cardiomyocytes.

RESULTS

Wnt/β-catenin signalling drives a core proliferative transcriptional programme in hPSC-CMs

The neonatal regenerative window in mice and pigs closes within the first week of postnatal development (Porrello et al., 2011; Ye et al., 2018; Zhu et al., 2018). Recent comparison of the neonatal and adult cardiac transcriptomes suggests that Wnt/β-catenin signalling is shut down postnatally concomitant with the closing of the regenerative window (Quaife-Ryan et al., 2017). Consistent with this finding, nuclear expression of active β-catenin (phosphorylated-Y489) was reduced during postnatal development of the mouse heart between postnatal day (P)1 and P7 and was virtually undetectable in P14 cardiomyocytes (Fig. 1A). Moreover, the total expressions of *Ctnnb1* and the main transcriptional effector of β-catenin, *Tcf7l2*, were also downregulated between P1 and P14 (Fig. 1B). These results suggest that the shutdown of postnatal Wnt/β-catenin activity is correlated with the loss of regenerative potential during heart development.

Wnt/β-catenin signalling was previously identified as a driver of hPSC-CM proliferation (Mills et al., 2017). In particular, the GSK3 inhibitor, CHIR99021 (CHIR), was identified as a potent cardiomyocyte mitogen in immature hPSC-CMs. We therefore sought to determine whether β-catenin is required to facilitate CHIR-induced cardiomyocyte proliferation in immature hCOs (Fig. 1C). β-Catenin has pleiotropic actions in the cell-cell cadherin junction and directs transcriptional responses by migrating into the nucleus. CHIR stimulated accretion of total β-catenin at intercalated discs but also increased nuclear localisation of active β-catenin (Fig. 1D,E). Similar to what was observed in mouse cardiomyocytes *in vivo*, *CTNNB1* was downregulated during human development (Fig. 1F). CHIR also led to an increase in cardiomyocyte proliferation in hCOs as evidenced by increased Ki-67 and pH3 staining (Fig. 1G,H).

We next investigated whether CHIR stimulated cardiomyocyte proliferation though β-catenin. Given that hCOs contain both cardiomyocytes and stromal cells (Mills et al., 2017; Voges et al., 2017), the cardiomyocyte-specific effects of CHIR were assessed using an *NKX2-5*^{eGFP} cell line followed by fluorescence-activated cell sorting (FACS) purification of cardiomyocytes (GFP^{+}) and stromal cells (GFP^{-}). *NKX2-5*^{eGFP} hCOs were treated with DMSO or CHIR, and the purity of isolated cell populations was validated by qPCR for *COL1A1* and *MYH6* (Fig. 1J,K). Using *AXIN2* as a read-out for β-catenin transcriptional activity, it was determined that CHIR increased *AXIN2* expression in hCO cardiomyocytes (Fig. 1L). The small molecule iCRT-14 inhibits the interaction between β-catenin and its transcriptional effector partner, TCF7L2 (Gonsalves et al., 2011). When hCOs were treated with CHIR and iCRT-14, *AXIN2* expression and Ki-67 staining were blunted (Fig. 1M,N). These results indicate that CHIR promotes cardiomyocyte cell-cycle activity through β-catenin/TCF7L2-depedent signalling.

To define the transcriptional networks regulated by canonical Wnt/β-catenin signalling in immature hPSC-CMs, we subjected purified hPSC-CMs and CD90^{+} stromal cells treated with CHIR to RNA-sequencing (RNA-seq). CHIR significantly regulated 1244 genes in cardiomyocytes and 689 genes in CD90^{+} stromal cells and co-regulated a network of 299 genes in both myocytes and stromal cells (Fig. 2A). In cardiomyocytes and stromal cells, CHIR downregulated specific transcriptional programmes controlling cell identity, such as cardiac muscle contraction and heart development in cardiomyocytes and cell matrix adhesion and regulation of cell migration in CD90^{+} stromal cells (Fig. 2B,C). CHIR induced a common suite of cell cycle-related transcriptional programmes in both cell populations (Fig. 2C). Collectively, these findings suggest that CHIR stimulates β-catenin/TCF7L2 signalling to drive partial loss of cellular identity whilst simultaneously promoting cell proliferation. Despite partial loss of cellular identity, principal coordinates analysis demonstrated that CD90^{+} stromal cells and cardiomyocytes remained transcriptionally distinct even after CHIR treatment (Fig. S1).

To ascertain which genes were the direct targets of β-catenin in human cardiomyocytes, chromatin immunoprecipitation-squencing (ChIP-seq) of TCF7L2 in CHIR-stimulated hPSC-CMs was performed (Fig. 2D). Enhancers and promoters of cardiomyocytes were also identified using ChIP-seq of H3K27ac and H3K4me3 histone marks, respectively. Pearson correlation of ChIP-seq indicated a high degree of reproducibility between replicates, but only peaks present in both samples were retained for subsequent analyses (Fig. 2E,F). As would be expected for enhancers, H3K27ac predominantly labelled loci >5 kb from the closest transcription start site (TSS; Fig. 2G). Genomic Regions Enrichment of Annotations Tool (GREAT) analysis suggested that these H3K27ac-labelled enhancers were closest to genes associated with the response to stress and cardiovascular system development (Fig. 2G). Alternatively, H3K4me3 peaks were located proximal to TSSs and, as expected, predominantly decorated gene promoters, which were associated with metabolic processes and cell-cycle regulation (Fig. 2G). H3K27ac and H3K4me3 ChIP-seq was further validated by assessing the peak location at well-characterised cardiomyocyte promoters and enhancers (Fig. S2). β-Catenin has previously been shown to bind predominantly to enhancers rather than promoters in cardiomyocytes (Iyer et al., 2018). In concordance with this finding, TCF7L2 peaks were located distant to TSS and occupied genes associated with glycosylphosphatidylinositol synthesis and nucleogenesis (Fig. 2G; Fig. S3). DNA-binding motif analysis indicated TCF/LEF motifs as the most enriched binding sites in the isolated TCF7L2-enhancer and TCF7L2-promoter peaks, thus validating the

Development (2020) 147, dev193417. doi:10.1242/dev.193417

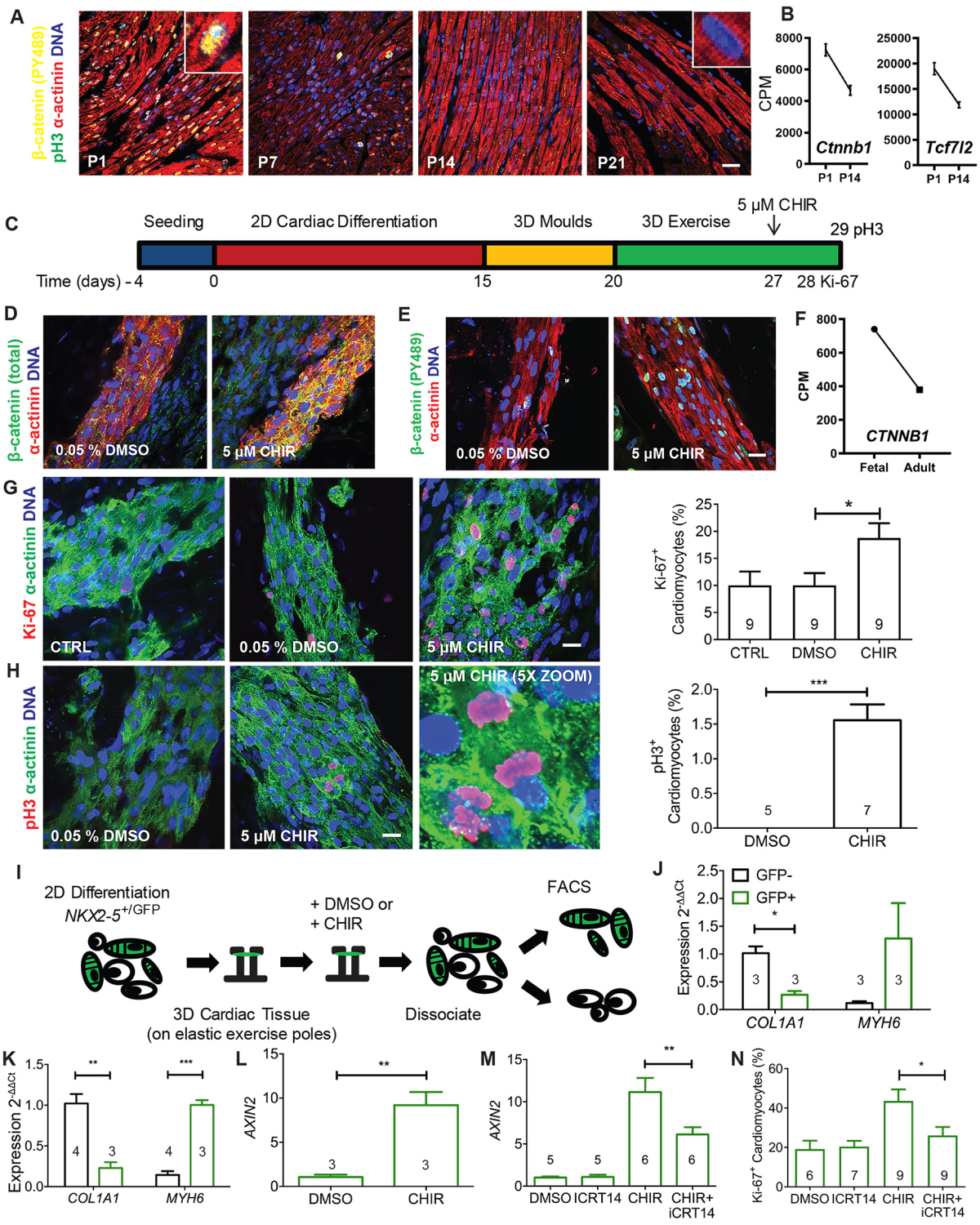

Fig. 1. See next page for legend.

TCF7L2-ChIP-seq dataset (Fig. 2H,I). These TCF7L2-occupied enhancers and promoters were associated with BMP signalling, mitochondrial replication and Wnt receptor signalling by the BMP pathway (Fig. 2J).

Next, the core β-catenin gene network was identified by isolating CHIR-regulated genes that were also direct targets of TCF7L2 in hPSC-CMs (Fig. 2K). Upregulated direct targets of β-catenin were strongly associated with the cell cycle. Downregulated genes were associated with the hypoxia response and the β-catenin destruction complex (Fig. 2K).

Wnt/β-catenin function is contingent on cardiomyocyte maturity during mouse development

During the first week of life, neonatal cardiomyocyte proliferation is rapidly shut down (Alkass et al., 2015). Delivery of cardiac mitogens during this period markedly augments cardiomyocyte

Development (2020) 147, dev193417. doi:10.1242/dev.193417

Fig. 1. Wnt/β-catenin is developmentally shut down in mouse heart and drives human ESC-derived cardiomyocyte proliferation. (A) Nuclear expression of β-catenin is concomitantly downregulated with pH3$^+$ proliferating cardiomyocytes during postnatal cardiac maturation in mice. (B) *Ctnnb1* and *Tcf7l2* are downregulated in cardiomyocytes during postnatal development between P1 and P14. Data were obtained from cardiomyocyte nuclei RNA-seq from Quaife-Ryan et al. (2017) (GSE95764). *n*=3 per group. Data are represented as counts per million (CPM). (C) Activation of β-catenin in human hCOs results in activation of cardiomyocyte proliferation. The GSK3 inhibitor CHIR was used to activate β-catenin in these experiments, and DMSO was used as a vehicle control. (D) Treatment of hCOs with CHIR resulted in retention of inactive β-catenin at cell-cell junctions. (E) Treatment of hCOs with CHIR resulted in active β-catenin in cardiomyocyte nuclei. (F) Human *CTNNB1* is downregulated during cardiac maturation *in vivo*. RNA-seq samples are available at GEO with accession GSE93841. (G) Treatment of hCOs with CHIR resulted in induction of proliferation in cardiomyocytes after 24 h using Ki-67. Data were pooled from two independent experiments. Statistical significance was tested using ANOVA with Dunnett's post-hoc test. We counted 4784 cardiomyocytes manually in these experiments. (H) Treatment of hCOs with CHIR resulted in induction of proliferation of cardiomyocytes after 48 h using pH3 as a marker of mitosis. Data were pooled from two independent experiments. We counted 2641 cardiomyocytes manually in these experiments. (I) Schematic diagram of strategy to purify cardiomyocytes from hCOs generated using the *NKX2-5*$^{GFP/+}$ human ESC line. (J,K) qPCR of target genes confirms separation of cell populations and purification of cardiomyocytes in the GFP$^+$ fraction in both DMSO- (J) and CHIR-treated (K) hCOs at 24 h. qPCR data are normalized to GFP$^-$ cells for *COL1A1* and to GFP$^+$ cells for *MYH6*. Data are from three or four independent experiments. (L) qPCR of the β-catenin transcriptional target *AXIN2* confirms transcriptional activation in cardiomyocytes (GFP$^+$ fraction) in CHIR-treated hCOs at 24 h. Data are from three or four independent experiments. (M) Inhibition of β-catenin transcriptional activity using iCRT14 is confirmed via qPCR of *AXIN2* in hCOs after 24 h. (N) iCRT14 inhibits CHIR induction of cardiomyocyte cell cycle in hCOs after 24 h. The numbers in bar graphs represent the number of hCOs analysed in each group. Scale bars: 20 µm in A,D,G,H. P1, 1-day-old mice; P7, 7-day-old mice; P14, 14-day-old mice; P21, 21-day-old mice. 2D denotes cardiac cultures grown on flat culture dishes. 3D denotes cardiac cultures formed into three-dimensional cardiac organoids.

proliferation, presumably because neonatal cardiomyocytes are in a proliferative state (D'Uva et al., 2015; Heallen et al., 2011). To determine whether Wnt/β-catenin drives cardiomyocyte proliferation in the neonatal cardiomyocyte proliferative window, a constitutively active form of β-catenin called N90Δ-CTNNB1 (caBCAT) was delivered to neonatal mice using adeno-associated virus-6 (AAV6-caBCAT) (Fig. 3A). Incorporation of 5-bromo-2′-deoxyuridine (BrdU) by cardiomyocytes was markedly increased in caBCAT-injected mice (Fig. 3B,C). Although heart weight was unaltered (Fig. 3D), the cross-sectional area of caBCAT-treated cardiomyocytes was significantly reduced (Fig. 3E). Moreover, the number of cardiomyocytes was increased by ∼16% in caBCAT-treated neonatal mice (Fig. 3F), consistent with bona fide induction of cardiomyocyte proliferation. Echocardiographic assessment of caBCAT-treated mice indicated that fractional shortening (FS) was slightly increased when compared with controls, although the ejection fraction (EF) was unaffected (Fig. 3G). To determine whether endogenous Wnt/β-catenin was required for neonatal cardiomyocyte proliferation *in vivo*, neonatal mice were treated with inhibitor of Wnt response 1 (IWR-1), which stabilises the β-catenin destruction complex and thereby inhibits Wnt/β-catenin signalling (Chen et al., 2009). IWR-1 treatment significantly reduced cell-cycle activity in the neonatal mouse heart as indicated by pH3 staining (Fig. 3H). Hence, Wnt/β-catenin signalling potentiates neonatal cardiomyocyte proliferation during the first week of postnatal development in mice.

β-Catenin was demonstrated to drive both neonatal mouse and immature hPSC-CM proliferation, but the adult heart is refractory to cardiomyocyte mitogens (Quaife-Ryan et al., 2016). We therefore assessed whether caBCAT was capable of potentiating adult cardiomyocyte proliferation in an adult mouse MI model (Fig. 4A). AAV6-caBCAT was benchmarked against the well-characterised pro-proliferative mitogen, YAP1 (Lin et al., 2014). For these experiments, a constitutively active form of YAP1, called YAP1-S127A (caYAP), was encapsulated in AAV6. Characterisation of AAV6 intracardiac injections showed transgene expression specifically at intracardiac injection sites and strong enrichment for gene expression in cardiomyocytes (Fig. S4). Both caBCAT and caYAP exhibited marked cardioprotective effects on cardiac function (Fig. 4B). Moreover, caBCAT significantly mitigated cardiac scarring after MI compared with GFP controls (Fig. 4C,D). FACS quantification of fibroblasts, leukocytes and endothelial cells at day 3 post-MI indicated that caBCAT expression diminished the number of fibroblasts (Fig. S5), suggesting that the β-catenin antifibrotic response is instructed during the early reparative phase post-infarction. However, in contrast to caYAP, which increased BrdU incorporation and exerted anti-hypertrophic effects in adult cardiomyocytes (Fig. 4E,G,H), caBCAT exerted similar cardioprotective effects independently of cardiomyocyte proliferation, because neither BrdU incorporation nor pH3 was elevated compared with controls (Fig. 4F-H). Hence, Wnt/β-catenin potentiates proliferation of immature hPSC-CMs and neonatal mouse cardiomyocytes but is insufficient to drive proliferation of adult cardiomyocytes despite its cardioprotective actions in the adult myocardium.

To understand how β-catenin facilitated cardioprotection rather than regeneration in the adult heart, RNA-seq was performed on cardiomyocytes isolated from caBCAT- or GFP-treated adult mice after MI (Fig. 5A). Principal coordinates analysis suggested good reproducibility between replicates (Fig. 5B). It was demonstrated previously that adult fibroblasts and leukocytes revert to a neonatal-like transcriptional state post-MI, whereas adult cardiomyocytes do not (Quaife-Ryan et al., 2017). Hence, we next assessed whether β-catenin could facilitate the acquisition of a neonatal-like transcriptional programme in adult cardiomyocytes. Comparison of the caBCAT and GFP transcriptional signatures with a previously published transcriptional resource of neonatal and adult mouse cardiomyocytes post-MI (Quaife-Ryan et al., 2017) revealed that neither group reverted fully to a neonatal-like transcriptional state post-MI (Fig. S6). However, a subset of caBCAT downregulated genes were associated with mitochondrial biogenesis, oxidative phosphorylation and the Warburg effect, in addition to the β-adrenergic hypertrophic response (*Ppargc1a*, *Nr4a3* and *Cebpb*) (Arany et al., 2005; Bhalla et al., 2014; Feng et al., 2015; Pearen et al., 2008) (Fig. 5C). *Klf15*, a known negative regulator of β-catenin signalling (Noack et al., 2012), was also downregulated by caBCAT treatment. Gene ontological (GO) analysis revealed that caBCAT downregulated genes were associated with catecholamine stimulation and the regulation of transcription (Fig. 5D). Interestingly, caBCAT appeared to induce inflammatory, angiogenic and apoptotic transcriptional responses in adult cardiomyocytes (Fig. 5D). Therefore, caBCAT stimulates a cardioprotective response associated with modulation of oxidative phosphorylation and inflammatory genes without inducing cell-cycle transcriptional networks in adult cardiomyocytes.

Understanding the differential Wnt/β-catenin response in regenerative and nonregenerative cardiomyocytes

Wnt/β-catenin signalling has distinct functions in proliferative cardiomyocytes (immature hPSC-CMs and neonatal myocytes) and

Development (2020) 147, dev193417. doi:10.1242/dev.193417

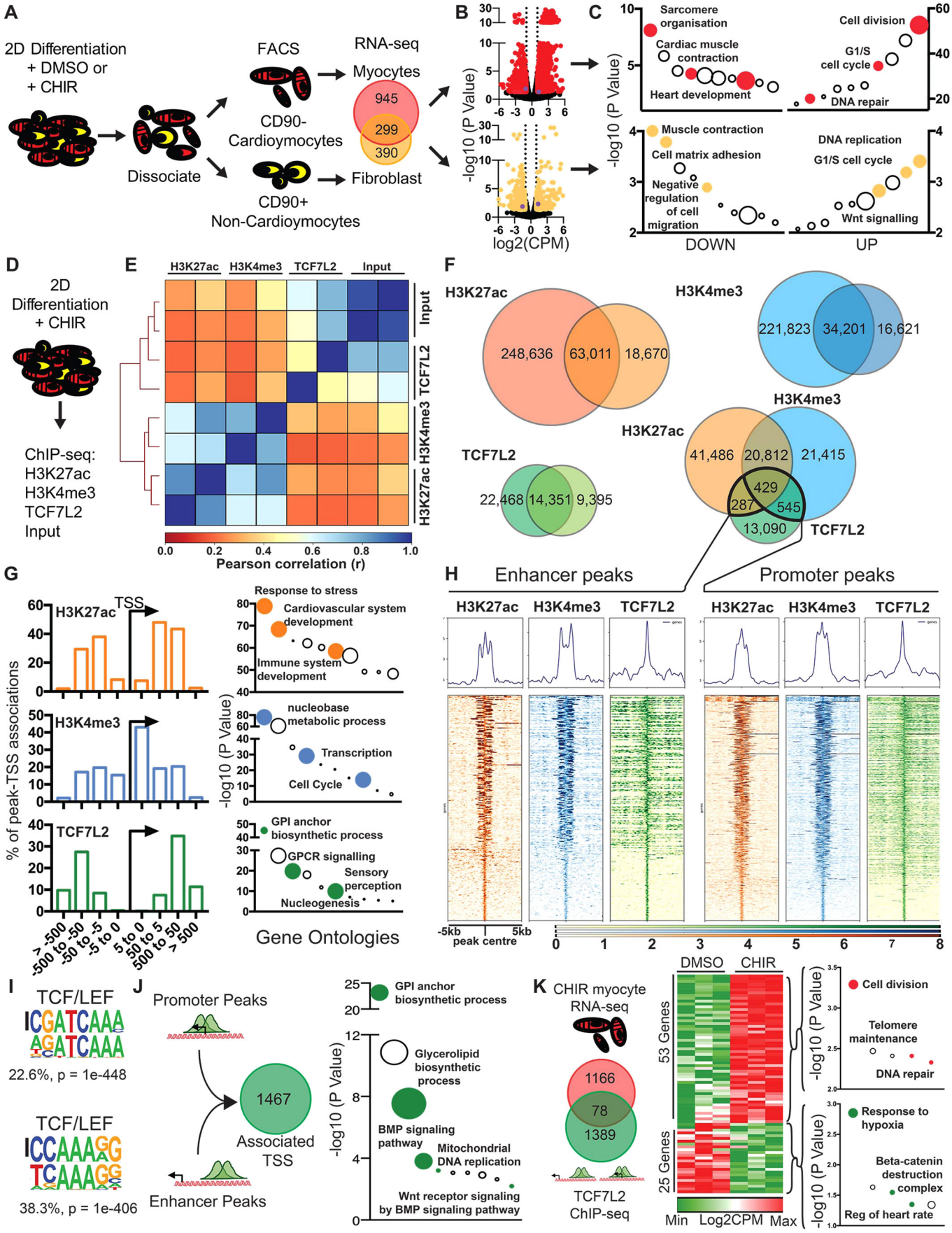

Fig. 2. See next page for legend.

Development (2020) 147, dev193417. doi:10.1242/dev.193417

Fig. 2. Defining the β-catenin signalling network in human ESC-derived cardiomyocytes. (A) Schematic outline for isolating and performing RNA-seq on cardiomyocytes and CD90$^+$ stromal cells from human cells differentiated in two-dimensional cardiac cultures and treated with CHIR or DMSO. This analysis identified a common network of 299 differentially expressed genes shared by cardiomyocytes and fibroblasts. *n*=3 experiments for all groups. (B) CHIR regulated 1244 cardiomyocyte genes (725 genes upregulated and 519 downregulated) and 689 fibroblast genes (298 upregulated and 391 downregulated). Significant genes are labelled in red or yellow for myocyte or stromal cells, respectively. Two genes were differentially regulated in cardiomyocytes and stromal cells (highlighted in purple). (C) Treatment with CHIR stimulated cell-cycle gene ontologies (GOs) in both myocytes and fibroblasts. Alternatively, GOs involved in cell identity, such as sarcomeric organisation and cell matrix adhesion, where shut down in myocytes and stromal cells, respectively. (D) Schematic diagram of ChIP-seq of H3K27ac, H3K4me3 and TCF7L2 in CHIR-treated 2D cardiac cells. Promoter and enhancer loci were identified in 2D-derived cardiomyocytes using H3K27ac and H3K4me3 ChIP-seq. *n*=2 experiments. (E) Consistency between sample groups was assessed using Pearson's correlation. (F) Venn diagrams of H3K27ac, K3K4me3 and TCF7L2 peaks. (G) The majority of TCF7L2 and H3K27ac peaks were situated distal to TSSs. H3K4me3 peaks were proximal to TSSs. GOs of genes associated with H3K27ac, H3K4me3 and TCF7L2 peaks are displayed. (H) The distribution of H3K27ac, H3K4me3 and TCF7L2 peaks at TCF7L2 enhancers and promotors. (I) *De novo* motif analysis identified two TCF/LEF binding motifs in TCF7L2 enhancer and promoter peaks. The black bar highlights the *de novo* motifs, and the associated known motif is beneath. The two motifs were found in 22.6% (top) and 38.3% (bottom) of peaks. (J) TCF7L2 enhancer and promoter peaks were associated with 1467 genes implicated in glycosylphosphatidylinositol synthesis, BMP signalling, mitochondrial DNA replication and Wnt/BMP signalling. (K) Of the 1244 CHIR differentially expressed genes, 78 were direct targets of TCF7L2. The 53 CHIR-upregulated TCF target genes were associated with cell cycle gene ontologies, and the 25 downregulated genes were associated with hypoxia and the β-catenin destruction complex.

nonproliferative cardiomyocytes (adult myocytes). To understand the context-dependent role of β-catenin during development, the β-catenin transcriptional response of proliferative myocytes and adult myocytes was compared. We first compared target genes of TCF7L2, CHIR-responsive genes and a published network of cardioregenerative genes (Quaife-Ryan et al., 2017) (Fig. 6A). A core network of 21 genes were shared between these datasets. The CHIR-responsive and cardioregenerative gene network displayed significant overlap, with 32.9% of the cardioregenerative genes also regulated by CHIR (Fig. 6A). By contrast, the CHIR-responsive and adult myocyte caBCAT responses were largely transcriptionally distinct (4.3% of MIP56.caBCAT genes were present in the CHIR dataset; Fig. 6B).

We next validated whether the core CHIR-regenerative network genes were downregulated when β-catenin signalling was inhibited in neonatal mouse hearts *in vivo* using IWR-1 (Fig. 6C). qPCR confirmed downregulation of a number of genes in the core CHIR-proliferative network after IWR-1 inhibition of β-catenin signalling in neonatal mice (Fig. 6C). These β-catenin target genes were highly downregulated in adult versus neonatal mouse cardiomyocytes (Fig. 6D). By contrast, the same set of genes was unaffected in adult hearts treated with caBCAT (Fig. 6C). It has been shown previously that the capacity of β-catenin to bind to its targets is dependent, in part, on the epigenetic status of target gene loci (Li et al., 2011; Wöhrle et al., 2007). However, the promoter regions of core genes in the CHIR-regenerative transcriptional network did not become progressively inaccessible during postnatal development (Fig. S7). Hence, the differential role of β-catenin in immature and mature cardiomyocytes appears to be facilitated by distinct gene programmes, which cannot be explained by the loss of chromatin accessibility at cardioregenerative target loci.

DISCUSSION

During postnatal development, cardiomyocytes undergo drastic transcriptional changes that result in cell-cycle arrest and, as a result, the adult heart becomes largely insensitive to mitotic stimuli (Gilsbach et al., 2018). Our previous multicellular transcriptomic analysis of mammalian heart regeneration predicted a core β-catenin-dependent transcriptional network associated with the neonatal cardiac regenerative state (Quaife-Ryan et al., 2017). Based on these findings, it was hypothesised that β-catenin signalling might be central to neonatal cardiomyocyte proliferation, and it was further proposed that reinduction of Wnt/β-catenin signalling could promote adult cardiomyocyte proliferation. Here, we demonstrate that the role of β-catenin is highly dependent on the developmental maturity of cardiomyocytes. β-Catenin potentiated proliferation of immature cardiomyocytes but led to cardioprotection in the adult heart post-MI without inducing cardiomyocyte proliferation.

The transcriptional targets of Wnt/β-catenin signalling in specific cardiac cell populations are not well defined. To characterise Wnt/β-catenin-dependent transcriptional networks further in human cardiac cells, we carried out transcriptional profiling of hPSC-CMs and stromal cells after inhibition of GSK3 with CHIR. As would be expected, canonical Wnt/β-catenin signalling was characterised by induction of a core network of cell cycle-related genes common to both cardiomyocytes and CD90$^+$ stromal cells. However, β-catenin signalling also elicited distinct gene programmes in these cell types, suggesting that the β-catenin transcriptional response is dependent, in part, on cellular identity. Moreover, CHIR-treated cardiomyocytes exhibited diminished sarcomeric gene expression, whereas CHIR-treated stromal cells displayed decreased expression of cell adhesion/extracellular matrix genes, consistent with partial loss of cell identity. Downregulation of contractile genes in cardiomyocytes treated with CHIR is consistent with previous observations that GSK3 inhibition diminishes cardiac contractility in hCOs and knockout mice (Mills et al., 2017; Zhou et al., 2016). Notably, GSK3 inhibition in hPSC-CMs treated with CHIR induced ∼35% of the neonatal mouse regenerative gene network identified by Quaife-Ryan et al. (2017). A core subset of 20 of these genes were also direct targets of β-catenin/TCF7L2 identified by ChIP-seq. Importantly, pharmacological inhibition of β-catenin in neonatal mice was associated with repression of several genes embedded within this core network. Overall, these findings define a common transcriptional programme, through which β-catenin promotes proliferation of immature human and mouse cardiomyocytes.

A key finding of the present study is that β-catenin has divergent roles in immature and mature cardiomyocytes. β-Catenin failed to promote adult cardiomyocyte proliferation but engendered a cardioprotective response and ameliorated scar size post-MI. The transcriptional responses of immature and mature cardiomyocytes to active β-catenin signalling displayed strikingly minimal overlap. Only ∼5% of adult β-catenin-regulated genes were also direct targets of β-catenin in hPSC-CMs. Moreover, these adult β-catenin-responsive genes were not differentially regulated by β-catenin inhibition in the neonatal mouse heart. Therefore, Wnt/β-catenin signalling is repurposed during postnatal cardiac development. Interestingly, this phenomenon occurs without changes in chromatin accessibility around the promoters of β-catenin target genes during postnatal cardiomyocyte maturation. One possibility is that β-catenin is redirected from regenerative to cardioprotective gene targets by complexing with distinct transcription factor binding partners in immature and mature cardiomyocytes. Future

Development (2020) 147, dev193417. doi:10.1242/dev.193417

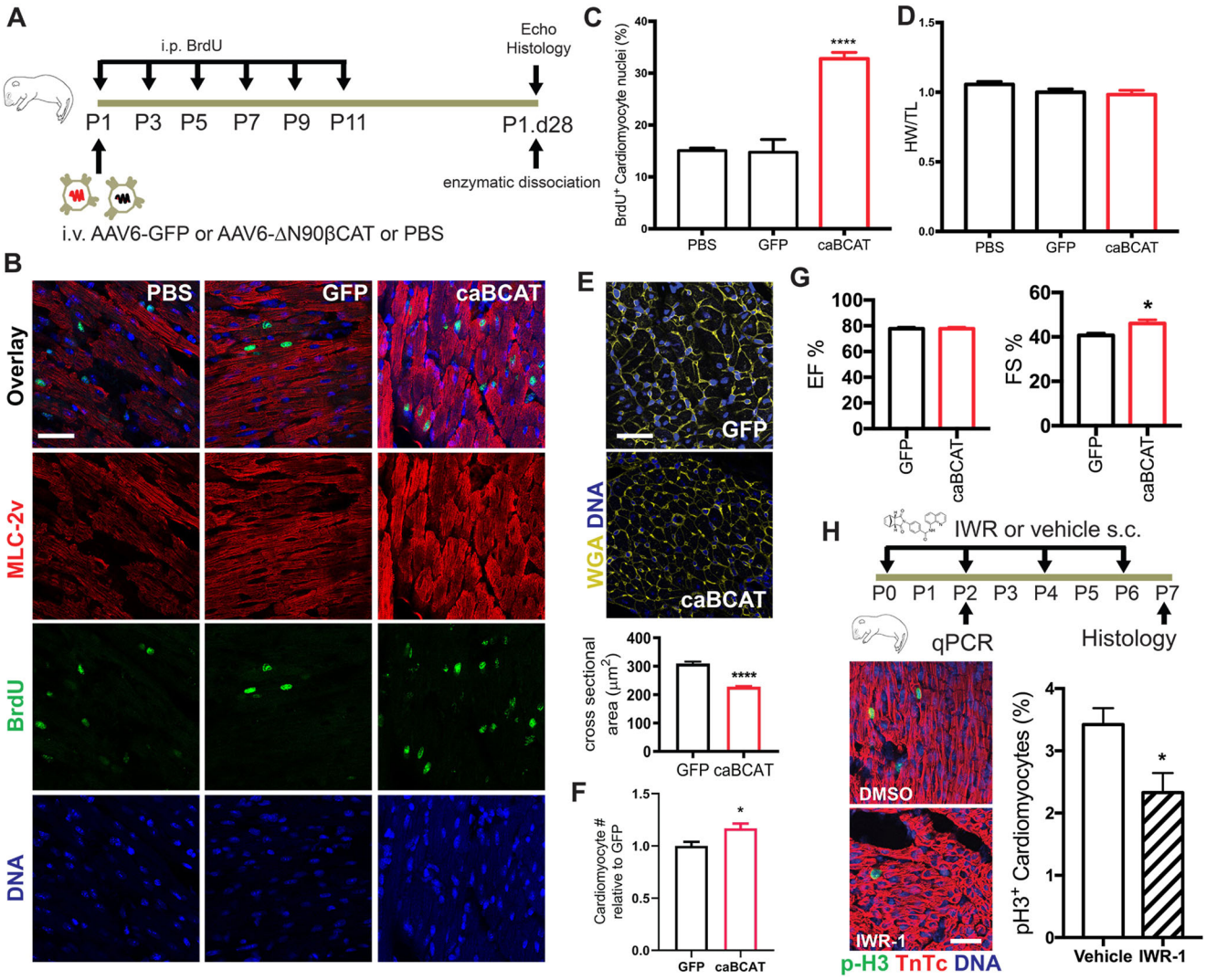

Fig. 3. Wnt/β-catenin signalling drives neonatal cardiomyocyte proliferation *in vivo*. (A) An experimental schematic diagram for i.v. injection of PBS-only control, AAV6-GFP and AAV6-caBCAT in neonatal mice. Mice were pulsed with 100 mg/kg of BrdU according to the schematic. (B) Representative images of BrdU staining of PBS-only-, GFP- or caBCAT-injected mice 28 days post-injection (P1.d28). (C,D) caBCAT induces neonatal cardiomyocyte DNA synthesis in P1.d28 animals (C) without a significant change in the ratio of heart weight (HW) to tibia length (TL) (D). (E) caBCAT-injected mice had reduced cardiomyocyte cell size. WGA, wheat germ agglutinin. (F) The number of cardiomyocytes was increased in caBCAT-treated mice at day 28 after neonatal AAV injection compared with GFP controls. (G) Cardiac function (ejection fraction, EF) was unaffected by caBCAT. FS, fractional shortening. (H) Top panel is an experimental schematic diagram of inhibition of β-catenin signalling with IWR-1 in neonatal mice. IWR-1 significantly reduced cardiomyocyte cell cycle ($pH3^+/TnTc^+$ cells) at P7. *n*=6 in both groups for B-E and G-H. *n*=10 caBCAT and *n*=11 GFP for F. Scale bars: 40 µm in B,E,H.

studies could validate this contention by identifying protein binding partners of nuclear localised β-catenin in neonatal and adult myocytes. Another possibility is that β-catenin-responsive enhancers are repurposed from pro-regenerative to protective functions during mammalian development, as has been reported recently for regeneration-responsive enhancers in zebrafish and killifish (Wang et al., 2020).

In contrast to the proliferative gene networks activated by β-catenin in immature cardiomyocytes, β-catenin promotes cardioprotection in the adult heart after MI without stimulating cardiomyocyte proliferation. By contrast, it should be noted that other studies have reported that Wnt/β-catenin signalling drives fibrosis in the adult heart by promoting extracellular matrix deposition from cardiac fibroblasts (Duan et al., 2012; Zhao et al., 2015). Our studies used AAV6, which is highly cardiomyocyte specific (Fig. S4). We showed that cardiomyocyte-specific expression of β-catenin was protective and that the antifibrotic effects of AAV6-BCAT were likely to occur secondary to cardioprotective effects in cardiomyocytes. Transcriptional analysis of caBCAT-treated adult hearts suggested that β-catenin signalling was associated with modulation of genes involved in inflammation and angiogenesis. However, it is important to note that the transcriptional responses of specific leukocyte or endothelial cell populations were not assessed in the present study, and it is unclear whether transcriptional changes resulting from β-catenin activation in myocytes influence inflammation and angiogenesis post-infarction. In addition, β-catenin was also found to modulate a number of genes related to cardiomyocyte metabolism in the adult heart. One such downregulated β-catenin-responsive gene in the adult heart was *Ppargc1a*, which is a master regulator of mitochondrial biogenesis that governs the transition from a glycolytic to an oxidative metabolic state in adult cardiomyocytes (Bhalla et al., 2014). Likewise, β-catenin also downregulated *Nr4a3*, which regulates the switch from glycolysis to oxidative

Development (2020) 147, dev193417. doi:10.1242/dev.193417

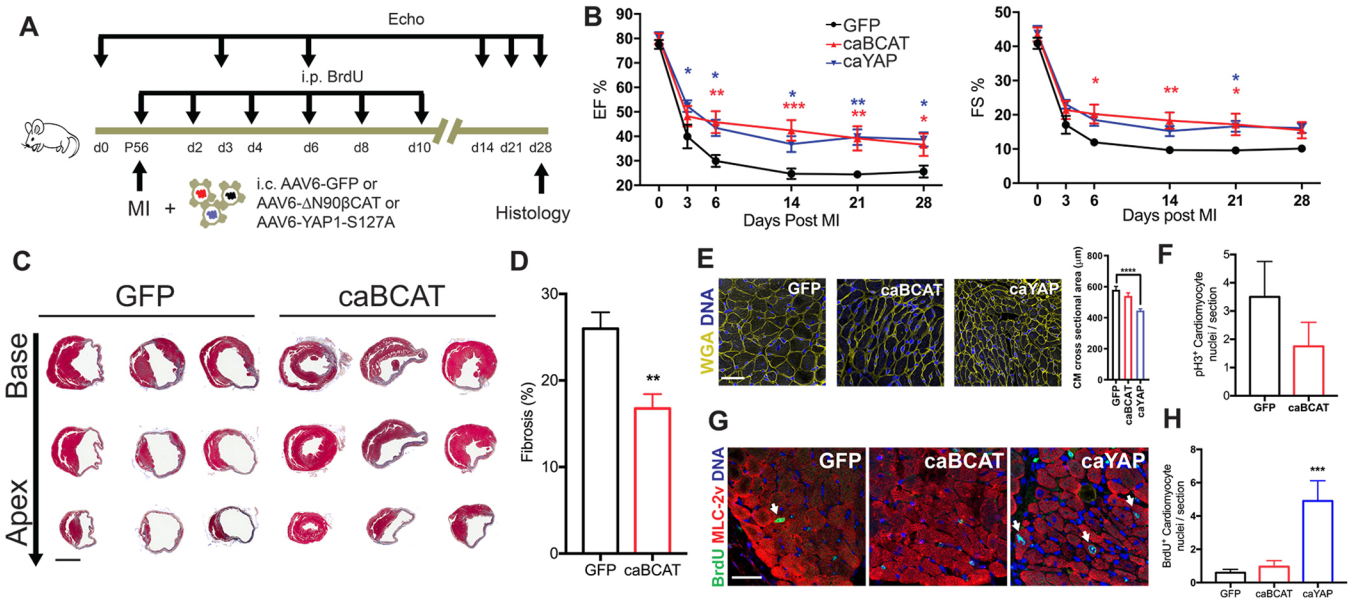

Fig. 4. Constitutively active β-catenin exhibits cardioprotective rather than pro-proliferative effects in the infarcted adult myocardium. (A) Schematic overview of AAV6-GFP, AAV6-caBCAT and AAV6-caYAP intramyocardial injection after MI in P56 adult mice (MIP56). Echocardiography was performed on days (d) 0, 3, 6, 14, 21 and 28 post-MI. BrdU (100 mg/kg) was injected every second day for 6 days. All mice were sacrificed at 28 days post-MI at P56 (MIP56.d28) for histology. (B) caBCAT and caYAP mitigated the decline cardiac function after MI as measured by ejection fraction (EF) and fractional shortening (FS). At 4 weeks post-infarction, EFs of GFP, caBCAT and caYAP groups were 26±2, 37±5 and 39±3%, respectively, and FS was 10±1, 16±2 and 16±1%, respectively. (C) Masson's Trichrome staining revealed a reduction in the infarct size of caBCAT-treated mice at 28 days post-injection. Representative images of three hearts from each group are displayed from base to apex. Scale bar: 1 mm. (D) Quantification of fibrotic tissue showed a significant reduction of fibrotic tissue in caBCAT-treated hearts. (E) Wheat germ agglutinin (WGA) staining and quantification of cardiomyocyte cross-sectional area in GFP-, caBCAT- and caYAP-treated mice at 28 days post-MI. The cross-sectional areas for 6200 cardiomyocytes were counted individually for this analysis (200 cardiomyocytes per heart). Scale bar: 40 μm. (F) Mitotic cardiomyocytes (pH3$^+$) were unaltered between GFP and caBCAT at MIP56.d3. (G) Representative images of BrdU$^+$/MLC-2v$^+$ cardiomyocytes in GFP, caBCAT and caYAP MIP56.d28 hearts. Scale bar: 40 μm. (H) Quantification of BrdU$^+$/MLC-2v$^+$ cardiomyocytes. caBCAT failed to increase the number of BrdU$^+$ cardiomyocytes. For B-E,G,H, *n*=10 AAV6-GFP, *n*=11 AAV6-caBCAT and *n*=10 AAV6-caYAP. For F, *n*=4 for both groups.

phosphorylation metabolism and induces hypertrophy of skeletal muscle (Feng et al., 2015; Pearen et al., 2008). Furthermore, caBCAT induced the expression of a key lactate transporter called Slc16a3 in adult cardiomyocytes. It has previously been shown that *Slc16a3* is widely expressed in glycolytic skeletal muscle (Uhlén et al., 2015) and highly expressed in glycolytic proliferative adult cardiomyocytes *in vivo* (Honkoop et al., 2019). Therefore, these observations might indicate that β-catenin sustains contractile function after cardiac injury by enabling usage of alternative fuel sources (glucose and lactate) for production of energy by adult cardiomyocytes. Further studies will be required to pinpoint the precise molecules that mediate such effects. Nevertheless, this β-catenin-induced metabolic programme is insufficient to drive adult cardiomyocyte proliferation.

This study demonstrates that β-catenin has distinct roles in immature and mature cardiomyocytes. β-Catenin drives a cell cycle-related gene network and promotes proliferation of immature neonatal cardiomyocytes and hPSC-CMs. By contrast, β-catenin is

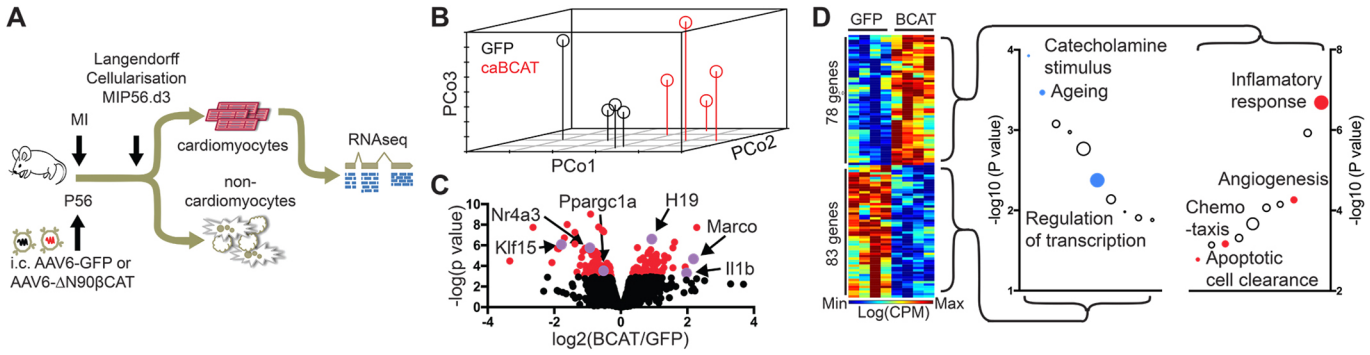

Fig. 5. The β-catenin cardioprotective gene programme in adult cardiomyocytes. (A) A schematic diagram detailing the isolation and RNA-seq of caBCAT-treated cardiomyocytes from mouse hearts post-MI. Mice were injected intramyocardially with either AAV6-GFP or AAV6-caBCAT at the time of MI surgery. After 3 days, cardiomyocytes were isolated and RNA-seq was performed. (B) Three-dimensional principal coordinates (PCo) analysis of caBCAT and GFP cardiomyocytes. Black, GFP-treated cardiomyocytes; red, caBCAT-treated cardiomyocytes. (C) caBCAT differentially regulated 161 genes. The volcano plot depicts genes differentially regulated between caBCAT- and GFP-treated cardiomyocytes. Significantly regulated genes are displayed in red, and genes of interest are highlighted in purple. (D) caBCAT upregulated 76 and downregulated 83 cardiomyocyte genes. Downregulated genes were associated with metabolic processes and transcription. Inflammatory and angiogenic genes were upregulated. *n*=4 for both groups.

Development (2020) 147, dev193417. doi:10.1242/dev.193417

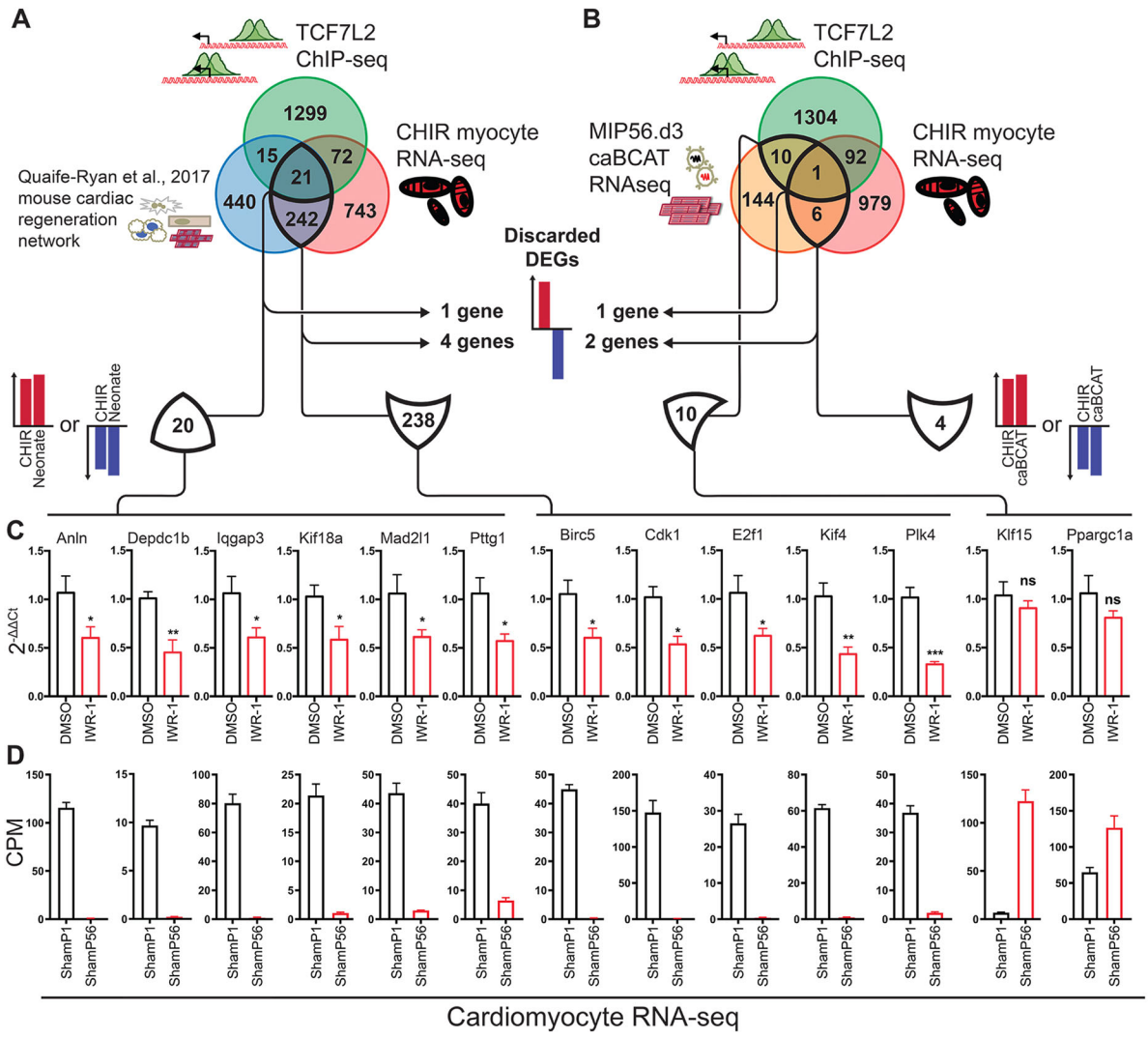

Fig. 6. β-Catenin drives distinct transcriptional programmes in regenerative and nonregenerative cardiomyocytes. (A) Direct targets of TCF7L2 in multiple datasets of cardiomyocytes; CHIR-regulated genes and genes from the cardioregenerative gene programme described by Quaife-Ryan et al. (2017) were compared. Two hundred and sixty-three genes were common to CHIR and regeneration networks, and 21 were direct targets of TCF7L2. Five genes were not regulated in the same direction (e.g. upregulated in the regeneration network but downregulated in CHIR) and were discarded. (B) One gene was a direct target of TCF7L2 and was co-regulated in both the CHIR- and caBCAT-treated adult cardiomyocyte networks. Genes that were not regulated in the same direction in caBCAT- and CHIR-treated myocytes were discarded. DEGs, differentially expressed genes. (C) Several regeneration network, CHIR-regulated genes and TCF7L2 direct targets were validated by qPCR in IWR-1-treated neonatal hearts, including several that were direct targets of TCF7L2. qPCR data are represented as $2^{-\Delta\Delta Ct}$; n=5 for DMSO and n=6 for IWR-1. (D) Many CHIR-responsive genes were downregulated during postnatal cardiomyocyte development. None of the adult caBCAT-regulated genes was downregulated in IWR-1-treated neonatal hearts, potentially because of low-level expression in neonatal cardiomyocytes. Data were obtained from RNA-seq of isolated neonatal (ShamP1) and adult (ShamP56) cardiomyocytes and are represented as CPM (GSE95755) (Quaife-Ryan et al., 2017). n=4 for both groups.

redirected from mitotic genes to inflammatory, angiogenic and glycolytic metabolism-related gene targets in the adult heart, which is associated with cardioprotective effects post-MI. Thus, β-catenin might metabolically reprogram adult cardiomyocytes via induction of a neonatal-like glycolytic metabolic programme. These findings suggest that Wnt/β-catenin drives distinct proliferative and metabolic networks in regenerative and nonregenerative cardiomyocytes, respectively, which might contribute towards the inability of the adult heart to regenerate after injury.

MATERIALS AND METHODS

Ethical approval for animal experiments

Ethical approval for neonatal and adult mouse procedures was obtained from The University of Queensland's Animal Ethics Committee (AEC approval #SBMS/101/13/NHMRC or #SBMS/AIBN/138/16/NHMRC/NHF) or from the QIMR Berghofer Medical Research Institute Animal Ethics Committee (AEC approval #A18603M). All animal research was performed in accordance with National Health and Medical Research Council *Guidelines to Promote the Wellbeing of Animals Used for Scientific Purposes*.

Neonatal mouse AAV injections

Timed pregnant CD-1 (MGI:5649524) female mice were housed in standard conditions, with 12 h/12 h light/dark cycles and *ad libitum* access to food and water. At P1, neonatal CD-1 mice were separated from their mother and were anaesthetised by being placing on ice for 1-2 min until they were motionless. The mice were then removed from the ice, positioned laterally, and an LED surgical lamp was used to transilluminate the superficial temporal vein. A Hamilton syringe with a 30-gauge needle was used to inject 20 µl of 1×10^{11} AAV6-caBCAT, 1×10^{11} AAV6-GFP or PBS into the

Development (2020) 147, dev193417. doi:10.1242/dev.193417

superficial temporal vein. The viruses were diluted in PBS. Correct needle placement was verified by observation of flushing of blood from the afferent segment of the vein. After virus injection, each pup was then rapidly warmed under a heat lamp until moving normally and returned to littermates. Once the entire litter had been injected, the pups were cleaned, rolled in the mother's bedding and returned to the mother's cage. For mice pulsed with BrdU, the mice then received an injection of BrdU [100 mg/kg, intraperitoneally (i.p.)] on the day of virus injection and were subsequently injected with BrdU every second day for six doses.

Neonatal mouse IWR-1 injections

At P1, CD-1 pups were separated from mother and injected subcutaneously (s.c.) with either 40 µg of IWR-1 (~20 mg/kg) or 8 µl of DMSO. After each pup in the litter had been injected, the pups were cleaned, rolled in the mother's bedding and returned to the mother simultaneously. Injections were continued daily until hearts were collected for analysis. For qPCR, neonatal mice received injections at P1 and P2 and were collected at P2.5. For immunofluorescence, mice were injected daily until P7 and collected at P7.5.

Adult mouse intracardiac AAV injections and MI

8-week-old adult CD-1 male mice were housed in standard conditions with *ad libitum* access to normal chow and water. The mice were anaesthetised in a stinger box with 2% isoflurane (Bayer), then intubated and ventilated with 0.25 l/min oxygen with a tidal volume of 250 µl and a respiration rate of 133 strokes/min (Minivent; Harvard Apparatus). Mice were positioned on a heated surgical mat to maintain body temperature. Once fully anaesthetised, the ventrolateral left chest was shaved, and a lateral thoracotomy was performed at the fourth intercostal space. The pericardium was separated using fine-nosed tweezers. A 7-0 Prolene suture was used to ligate the left anterior descending coronary artery permanently. MI was verified by observation of blanching of the myocardium. A Hamilton syringe with a 30-gauge needle was used to inject 1×10^{11} AAV particles (i.e. caYAP, caBCAT or GFP control). Viruses were diluted in sterile PBS to a final injection volume of 20 µl for all injection groups; four separate injections of 5 µl were injected around the infarct penumbra. After injection, the chest wall was closed using 4-0 silk suture and the overlying skin sutured with 6-0 Prolene suture. The mice were given an s.c. injection of buprenorphine (0.1 mg/kg) and carprofen (10 mg/kg) and allowed to recover. Starting from the day of the surgery, mice received BrdU injections (100 mg/kg, i.p.) every second day for six doses.

Adeno-associated virus construction

Sequences for caBCAT and caYAP were obtained from Addgene with the accessions 31787 and 42239, respectively. caBCAT was originally generated by deletion of the N-terminal 90 amino acids of human *CTNNB1* (Tward et al., 2007). caYAP contained a serine to alanine mutation of residue 127 of human *YAP1* (von Gise et al., 2012). caBCAT and caYAP were subcloned into pAAV-cDNA-V5His (Vector Biolabs) and encapsulated in AAV6 by Vector Biolabs. All constructs used a CMV promoter. AAV6-GFP was obtained from Vector Biolabs (Cat. # 7008).

Echocardiography

Echocardiography for neonatal mice injected i.v. with AAV6-caBCAT or AAV6-GFP was performed on day 28 post-injection. For adult MI experiments, echocardiography was performed on days 0 (day of surgery), 3, 7, 21 and 28. Mice were anaesthetized by inhalation of 2% isoflurane (Bayer) at a flow rate of 0.25 l/min oxygen. The mice were then arranged supine on a heated mat. The ventrolateral left chest was shaved, and then prewarmed ultrasound fluid was distributed on the chest. M-mode transverse images of the heart were obtained using an HD15 Philips ultrasound machine. The FS and EF were calculated using HD15 software on measurements obtained from these images. The mice were then removed from isoflurane and monitored until they made a full recovery.

Isolation of adult cardiac cell populations for FACS and RNA-seq

Three days after MI surgery, adult CD-1 mice were terminally anaesthetized with an i.p. injection of ketamine (100 mg/kg) and xylazine (12.5 mg/kg). The hearts were excised and washed in perfusion buffer (120.4 mM NaCl, 14.7 mM KCl, 0.6 mM KH_2PO_4, 0.6 mM Na_2HPO_4, 1.2 mM $MgSO_4.7H_2O$, 4.6 mM $NaHCO_3$, 10 mM Na-HEPES, 30 mM taurine, 5.5 mM glucose and 10 mM 2,3-butanedione 2-monoxime). A 21-gauge cannula was inserted into the aorta, taking care not to insert it through the aortic valve, and secured with 3-0 silk suture. The cannulated hearts were suspended on a Langendorff apparatus and retroperfused at a rate of 4 ml/min with oxygenated perfusion buffer at a temperature of 37°C. Once extraneous tissue and atria were removed, digestion buffer [200 µg/ml Liberase DH (Roche) in perfusion buffer] was retroperfused through the heart for ~8 min. The hearts were cut into small pieces (1-2 mm^3) with fine scissors in perfusion buffer and triturated with a 10 ml pipette. Heart cells were transferred through a 100 µm cell strainer and centrifuged at 30 ***g*** for 3 min at room temperature. The non-myocyte-enriched supernatant was used to isolate fibroblasts, leukocytes and endothelial cells using FACS. The myocyte pellet was washed with perfusion buffer, re-centrifuged and processed for RNA-seq.

FACS of non-myocyte cardiac cells

FACS was performed according to a previously published protocol (Quaife-Ryan et al., 2017). Isolated non-myocyte cells were resuspended in 100 µl of 5% bovine serum albumin (BSA)/PBS solution (137 mM NaCl, 2.7 mM KCl, 1.8 mM KH_2PO_4, 10 mM Na_2HPO_4 and 75 µM BSA). The cells were then incubated at 4°C for 20 min with CD90-APC (1:33, A14727; Thermo Fisher Scientific), CD45-FITC (1:10, 130-102-778; Miltenyi Biotec), CD31-BV421 (1:33, 102423; BioLegend) and Podoplanin-PE/Cy7 (1:66, 127411; BioLegned) in 100 µl of 5% BSA/PBS. The cell isolates were washed in 5% BSA/PBS solution and sorted with a BD FACS ARIA cell sorter. The purified cell populations were centrifuged at 1000 ***g*** for 5 min. The supernatant was removed, and cell pellets were resuspended in 1 ml TRIzol. See Table S1 for antibodies.

Generation of hPSC-CMs

Ethical approval for the use of human embryonic stems cells (ESCs) was obtained from The University of Queensland's Medical Research Ethics Committee (2014000801). All cell lines were tested for contamination and karyotypic abnormalities. Cardiomyocytes were produced using published protocols (Mills et al., 2019; Tiburcy et al., 2017; Voges et al., 2017). Briefly, cardiomyocyte/stromal cell cultures were produced from HES3 hESCs (WiCell) maintained using mTeSR-1 (STEMCELL Technologies). The hESCs were seeded at 2×10^4 cells/cm^2 in Matrigel-coated flasks, cultured for 4 days using mTeSR-1 and passaged with TrypLE (Thermo Fisher Scientific). Subsequently, hESCs were differentiated into cardiac mesoderm by culturing for 3 days in RPMI B27- medium [RPMI 1640 GlutaMAX +2% B27 supplement minus insulin (Thermo Fisher Scientific), 200 µM L-ascorbic acid (Sigma-Aldrich) and 1% penicillin/streptomycin (Thermo Fisher Scientific)] and growth factors: 5 ng/ml BMP-4 (R&D Systems), 9 ng/ml Activin A (R&D Systems), 5 ng/ml FGF-2 (R&D Systems) and 1 µM CHIR99021 (STEMCELL Technologies; Cat. # 72054). The medium was exchanged daily. Cardiomyocyte specification was completed by 3 days of culture in RPMI B27- media with 5 µM IWP-4 (STEMCELL Technologies), followed by another 7 days of culture with RPMI B27+ [RPMI 1640 GlutaMAX +2% B27 supplement with insulin (Thermo Fisher Scientific), 200 µM L-ascorbic acid (Sigma-Aldrich) and 1% penicillin/streptomycin (Thermo Fisher Scientific)]. The cardiac cells, comprising ~75% cardiomyocytes and ~25% $CD90^+$ stromal cells (Voges et al., 2017), were dissociated at 15 days using human cardiac digestion buffer [0.2% collagenase type I (Sigma-Aldrich) in 20% fetal bovine serum (FBS) in PBS (with Ca^{2+} and Mg^{2+})] for 45 min at 37°C. The cardiac cells were digested further with 0.25% trypsin-EDTA for 10 min. The cells were strained through a 100 µm filter, centrifuged at 300 ***g*** for 3 min, and resuspended at the required density for three-dimensional culture in CTRL medium [α-MEM GlutaMAX (Thermo Fisher Scientific), 10% FBS, 200 µM L-ascorbic acid (Sigma-Aldrich) and 1% penicillin/streptomycin (Thermo Fisher Scientific)].

Development (2020) 147, dev193417. doi:10.1242/dev.193417

Large hCO fabrication and culture

For large hCOs, cardiac cultures were differentiated for 15 days from either HES3 or HES3 *NKX2-5*$^{eGFP/w}$ (Elliott et al., 2011) cell lines, and hCOs were fabricated using published methods (Voges et al., 2017). For each hCO, 5×10^5 cardiac cells in CTRL medium were mixed with collagen I to make a 150 µl final solution containing 1 mg/ml collagen I. Collagen I was then salt-balanced with 10× DMEM (Thermo Fisher Scientific) and pH neutralised with 0.1 M NaOH before mixing with Matrigel and cells. The mixture was prepared on ice and pipetted into circular PDMS moulds (Sylgard 184; Dow Corning). The collagen was allowed to gel at 37°C for 1 h before adding CTRL medium to cover the tissues (~3 ml/hCO). The hCOs were cultured for 5 days in moulds, with a change of medium every 2 days. The hCOs were transferred onto PDMS exercise poles and cultured for a further 7 days with a change of medium every 2-3 days. On day 27, hCOs were treated with DMSO (Sigma-Aldrich) (0.15%), 5 µm CHIR99021 (STEMCELL Technologies), iCRT14 (50 µM; Tocris) or CHIR+iCRT14 and collected for analysis at 24 or 48 h.

FACS of hPSC-CMs

Two-dimensional (2D) monolayers of cardiac cells after 15 days of culture were treated with either 0.05% DMSO or 5 µM CHIR for 24 h before dissociation. For hCOs, dissociation was performed using human cardiac digestion buffer for 45 min at 37°C, followed by 0.25% trypsin-EDTA for 10 min. The digested cells were then passed through a 100 µm mesh cell strainer (BD Biosciences) and centrifuged at 300 ***g*** for 3 min. Cells were incubated with primary antibodies (see Table S1) for 15 min at 4°C in FACS buffer (5% FBS in PBS), washed and then incubated with secondary fluorophore antibodies (see Table S1) in FACS buffer for 15 min at 4°C. The cells were then washed and resuspended in PBS for FACS. Live cells were gated on forward and side scatter, and doublets were excluded based on forward- and side-scatter width and height. $CD90^+$ and $CD90^-$ cells from human cardiac cultures were previously demonstrated to be stromal cells and cardiomyocytes, respectively (Voges et al., 2017).

RNA isolation, complementary DNA generation and qPCR

RNA was isolated from tissues or cells using TRIzol (Thermo Fisher Scientific) according to the manufacturer's instructions, unless otherwise specified. For whole tissues, tissues were homogenised in 1 ml of TRIzol and left at room temperature for 3 min to dissociate nucleoprotein complexes fully. Two hundred microlitres of chloroform was added, and the samples were vortexed for 30 s, incubated for 3 min at room temperature and centrifuged at 12,000 ***g*** for 15 min at 4°C. The aqueous phase containing RNA was transferred to a new Eppendorf tube. One millilitre of isopropanol was added, and 1 µl of GlycoBlue (Thermo Fisher Scientific) was used as a precipitant. The RNA pellet was washed in 75% ethanol/25% nuclease-free water, allowed to dry, resuspended in 87.5 µl of nuclease-free water and incubated at 55°C for 15 min.

For generation of complementary DNA (cDNA), RNA was first treated with RNase-free DNase (QIAGEN) and then column isolated using the RNeasy MinElute Clean-up kit (QIAGEN) according to the manufacturer's instructions. RNA was eluted from MinElute columns with 20 µl of nuclease-free water. RNA was then used for qPCR or RNA-seq.

The Superscript III first-strand synthesis system (Invitrogen) was used to generate cDNA. DNase-treated RNA was prehybridised with 1 µl (150 ng) of random hexamer primers and 1 µl of 10 mM dNTPs at 65°C for 5 min and placed on ice. The SuperScript reaction mix was added [4 µl of 5× first strand buffer, 1 µl of 0.1 mM dithiothreitol and 1 µl of RNase OUT (Thermo Fisher Scientific) and 1 µl of SuperScript III (Thermo Fisher Scientific)]. Reverse transcriptase-free controls had all the same reagents but without SuperScript III. The cDNA was generated using a thermocycler at 25°C for 10 min, 50°C for 60 min and 70°C for 15 min.

qPCR was performed using SYBR Green PCR Master Mix (Thermo Fisher Scientific) or PowerUp SYBR Green (Thermo Fisher Scientific) according to the manufacturer's recommendations. Primers were designed using NCBI Primer-BLAST (Ye et al., 2012) with the following parameters: PCR product size >80 and <150 bp, melting temperature=~59°C; if possible, primers spanning exon-exon junctions and target specificity were assessed against the Refseq mRNA database. qPCR was performed with a QuantStudio 5 system (Applied Biosystems) according to the manufacturer's instructions. Endogenous controls for mouse and human were either 18S ribosomal RNA or hypoxanthine-guanine phosphoribosyltransferase (*Hprt* or *HPRT1*) as specified. Primer sequences for qPCR are listed in Table S2.

ChIP-seq of hPSC-CMs

2D monolayers of hPSC-CMs were treated for 24 h with 5 µM CHIR. hPSC-CMs were fixed for 10 min at room temperature with 1% paraformaldehyde (PFA) in CTRL medium. Cross-linking was stopped by addition 0.125 M glycine for 5 min. Cells were washed 2× with ice-cold PBS and then scraped in 1 ml PBS into a 1.5 ml Eppendorf tube. Fixed cells were spun (200 ***g***, 10 min) and treated with lysis buffer according to the MAGnify Chromatin Immunoprecipitation kit protocol (150 µl/3 million cells assuming 15×10^6 cells/flask). Chromatin was sheared using a Bioruptor UCD2000 sonicator with the following settings: 12 cycles of 30 s sonication with 90 s cooling. Chromatin was sonicated in 1.5 ml Eppendorf tubes, and the volume of cell lysate in each tube during sonication was kept at 150 µl. Sheared chromatin in lysis buffer was stored at −80°C before ChIP. The ChIP reactions were carried out with MAGnify Chromatin Immunoprecipitation System (Thermo Fisher Scientific) reagents according to the manufacturer's instructions. Antibodies used in ChIP reactions were: 1 µg anti-TCF4 (1:30, Santa Cruz Biotechnology; sc-8631 X), 3 µl anti-H3K4me3 (1:50, Active Motif; 39159) and 5 µg anti-H3K27ac (1:30, Active Motif; 39133). ChIP-seq libraries were created with the TruSeq ChIP Library Preparation Kit (Illumina), with DNA size selected and quality controlled by Pippin Prep size selection (Sage Science). Libraries were read with the HiSeq SR Cluster v4 kit (Illumina) on a HiSeq 2500 sequencer with 50 bp single-end reads. Quality control data are summarized in Table S3.

RNA-seq of CHIR-treated hPSC-CMs and $CD90^+$ stromal cells

Libraries were constructed with the Ovation RNA-Seq system v.2 (for single primer isothermal amplifications and cDNA generation) coupled with the Ovation Ultralow System (NuGEN). Seven rounds of amplification were performed. The quality of libraries was ascertained using Qubit. Libraries were read with 50 bp SR Rapid Mode on a HiSeq1500 (Illumina).

RNA-seq of isolated adult AAV-BCAT and AAV-GFP cardiomyocytes

Once purified RNA was obtained, ribosomal RNA was depleted with Ribo Zero Gold (Illumina), RNA quality was verified using a MultiNA bioanalyzer (Shimadzu), and cDNA was generated with SuperScript II Reverse Transcriptase (Thermo Fisher Scientific). RNA-seq libraries were generated with TruSeq Stranded Total RNA kits (Illumina) and read with the HiSeq SR Cluster v.4 kit (Illumina) on a HiSeq 4000 sequencer (Illumina). RNA-seq mapping quality control data are listed in Table S4.

Cellularisation of fixed hearts for cardiomyocyte cell counting

Cardiomyocytes were isolated 28 days after P1 i.v. AAV injection (P1.d28), according to a previously published protocol (Bywater et al., 2020). Hearts were isolated from P1.d28 mice, washed with PBS and fixed in 1% PFA overnight at 4°C. The next day, the hearts were washed four times in PBS. The atria were removed, and the ventricles were diced into 1-2 mm^3 pieces and incubated with 0.5 U/ml collagenase B (Roche; Cat. # 11088807001) in 0.2% NaN_3/PBS and oscillated (1000 rpm) at 37°C. The supernatants containing cardiomyocytes were collected every 12 h and kept at 4°C in 0.2% NaN_3/FBS. Once dissociation was complete, the cardiomyocytes were centrifuged at 1000 ***g*** for 3 min, washed twice in PBS and stored in 0.2% NaN_3/PBS at 4°C. The cardiomyocytes were then counted on a haemocytometer.

Histology

Unless otherwise specified, animals were euthanised and tissues were briefly washed in PBS and fixed in 4% paraformaldehyde/PBS on a shaker overnight. The tissues were washed in PBS and processed for paraffin-embedded sectioning. Fixed heart tissues were cut transversely, dehydrated in sequential graduated ethanol washes, washed twice in xylene and embedded in paraffin wax cassettes. Tissues were then sectioned at 6 µm and mounted on SuperFrost Ultra Plus slides (Thermo Fisher Scientific). For

Development (2020) 147, dev193417. doi:10.1242/dev.193417

Masson's Trichrome staining, sections were deparaffinized and rehydrated in ethanol, washed in distilled water, stained in Weigert's Iron Haematoxylin for 10 min and washed in distilled water for 10 min. Sections were then stained in Biebrich Scarlet-Acid Fuchsin solution for 10 min and washed again in distilled water. Fibrotic tissue was differentiated in phosphomolybdic-phosphotungstic acid solution for 10 min and directly transferred to Aniline Blue solution for 0.5-3 min (depending on the strength of the Aniline Blue dye). The sections were washed in distilled water until the water ran clear and then further differentiated in 1% acetic acid/distilled water solution for 3 min. Sections were washed in distilled water, dehydrated in sequential graduated ethanol washes, cleared with xylene and mounted with DPX mounting medium (Sigma-Aldrich).

Whole-mount immunostaining of hCOs

hCOs were fixed with 1% PFA/PBS solution for 60 min at room temperature. The hCOs with PBS 3 times and stained with primary antibodies (Table S1) in blocking buffer, 5% FBS and 0.2% Triton X-100 (Sigma-Aldrich) in PBS overnight at 4°C. Cells were then washed in blocking buffer two times for 2 h and subsequently incubated with secondary antibodies (Table S1) and Hoescht (1:1000) overnight at 4°C. They were washed in blocking buffer two times for 2 h and imaged *in situ* or mounted on microscope slides using Fluoromount-G (Southern Biotech).

Immunofluorescent staining of mouse heart sections

Hearts were fixed in 4% PFA in PBS overnight, washed in PBS and halved with a single transverse cut at the ligature mark or, for non-infarcted mice, equidistant from the base and the apex. The hearts were dehydrated and embedded in paraffin wax. Each sample was sectioned at 6 µm thickness. Sections were rehydrated, blocked with 10% goat serum in PBS and stained with primary antibodies (see Table S1) in 2% goat serum/PBS overnight at 4°C. Sections were washed with PBS, stained with secondary antibodies and Hoechst 33342 (Life Technologies) diluted 1:1000 in 2% goat serum/PBS for 1 h at room temperature and mounted in FluoMount (Thermo Fisher Scientific). Each slide was imaged using a Leica DMi8 confocal microscope. For analysis of adult cardiomyocyte proliferation, four cross-sections for each heart were quantified. The number of positively stained cardiomyocytes was normalised per section. Each section was separated by 250 µm. For neonatal proliferation analysis, ten images from two sections from each heart were quantified. The number of positive cardiomyocytes was normalised to the total number of cardiomyocytes in each image.

Bioinformatics for RNA-seq analysis

Poor quality sequence (<30 Phred score) and adapters were clipped using Trimmomatic (v.0.36.6) (Bolger et al., 2014). Reads were mapped to either the human or mouse GRCh38/hg38 reference genome using STAR (v.2.4.0g1) (Dobin et al., 2013). HTSeq-count (Anders et al., 2015) on union mode was used to generate count matrices. Differential expression analysis was performed with EdgeR (v.3.2.4) (Robinson et al., 2010). For CHIR RNA-seq, differential analysis was performed with the EdgeR command glmLRT [log2(fold change) set to >1 or <−1, FDR<0.05]. For adult mouse post-MI myocyte RNA-seq, differential analysis was performed with the EdgeR command glmLRT [FDR<0.1]. GO analysis was performed using DAVID (Huang et al., 2007). Principal coordinates analysis was performed with the plotMDS function in EdgeR. Heatmaps were assembled with GENE-E (Broad Institute). See Table S5 for all bioinformatic tools used in the present study.

Bioinformatics for hPSC-CM ChIP-seq analysis

Trimmomatic (v.0.36.6) (Bolger et al., 2014) was used to trim adapter and poor-quality sequences (<20 Phred score). Reads were then mapped with Bowtie2 (v.2.3.4.1) (Langmead and Salzberg, 2012) to the reference human genome sequence GRCh37/hg19. Peaks were called with the callpeak function of MACS2 (v.2.1.1.0) (Zhang et al., 2008) with default parameters (q-value<0.01). For histone marks, broadpeaks were called using broad subcommand with broad.cutoff=0.1. Replicate peaks were intersected using the intersect function of GenomicRanges (v.1.34.0) (Lawrence et al., 2013). All ChIP-seq heatmaps and correlations were generated with deepTools2 (v.2.5.1.1.0) (Ramírez et al., 2016). GO analysis of ChIP-seq peaks was performed by associating the closest known transcription start sites with GREAT (v.3.0.0) (McLean et al., 2010). Motif binding site analyses were performed with the findMotifsGenome function in Homer (v.4.10) (Heinz et al., 2010). See Table S5 for all bioinformatic tools used in the present study.

Bioinformatic comparison of human and mouse RNA-seq and ChIP-seq datasets

Ensemble identities for orthologous genes between human and mouse were obtained using the biomaRt (v.2.38.0) (Durinck et al., 2009) package in R. Venn diagrams were then used to identify co-regulated genes between the datasets.

Other RNA-seq datasets used in analyses

Data used in some comparative analyses were obtained from Quaife-Ryan et al. (2017) or Mills et al. (2017) as indicated. The 'neonatal regenerative gene network' used in these analyses was obtained from Quaife-Ryan et al. (2017) (GSE95755). We demonstrated previously that adult cardiomyocytes and endothelial cells do not reactivate a neonatal proliferative programme after myocardial infarction (Quaife-Ryan et al., 2017). The 'neonatal regenerative gene network' used in Fig. 6 contains genes that were highly expressed in neonatal regenerating cardiac cells but were not deployed by adult cardiomyocytes and endothelial cells post-MI. This gene network was replete with cell-cycle genes and was bioinformatically predicted to drive proliferative responses in the regenerating heart (Quaife-Ryan et al., 2017). We subsequently demonstrated that induction of *c-Myc/pTEFb* transcription reactivated this neonatal regenerative gene network in adult cardiomyocytes (Bywater et al., 2020). Original datasets are available at the Gene Expression Omnibus (GEO) using accessions GSE93841 (human fetal and adult heart RNA-seq), GSE95755 (mouse regenerative gene network RNA-seq) and GSE95764 (cardiomyocyte nuclei RNA-seq and ATAC-seq).

Non-bioinformatic statistical analysis

Student's two-tailed unpaired *t*-test was used for comparisons between two groups. For comparison of more than two groups, a one-way ANOVA followed by Tukey's multiple comparisons post-hoc test was used. A two-way ANOVA with Tukey's post-hoc test was used to test multiple groups with two or more independent variables. In all figures, *P<0.05, **P<0.01, ***P<0.001 and ****P<0.0001. All data are mean±s.e.m. unless otherwise specified. Further information on the statistical analysis is presented in the figure legends. For mouse studies, n represents the number of mice. For human PSC-derived cardiac cell experiments, n represents individual experiments.

Acknowledgements

We thank V. Nink and G. Osbourne for their assistance with FACS at the Flow Cytometry facility at the Queensland Brain Institute, QFAB bioinformatics and I. Makunin at Galaxy Australia (https://usegalaxy.org.au/) for bioinformatics training, the Developmental Studies Hybridoma Bank for antibodies, and the Monash Health Translational Precinct Medical Genomics Facility and Australian Genome Research Facility for sequencing. We also thank A. Masel and C. Winterford at the QIMR Berghofer histology facility for assistance with immunostaining. Some of the data in this paper form part of G.A.Q.-R.'s PhD thesis, which was published online in 2020 by The University of Queensland (doi:10.14264/uql.2020.927).

Competing interests

G.A.Q.-R., R.J.M., J.E.H. and E.R.P. are co-inventors on patents for hCO maturation and cardiac regeneration held by The University of Queensland and QIMR Berghofer Medical Research Institute. J.E.H. is a co-inventor on licensed patents held by the University of Goettingen. R.J.M., E.R.P. and J.E.H. are co-founders, scientific advisors and stockholders in Dynomics.

Author contributions

Conceptualization: G.A.Q.-R., J.E.H., E.R.P.; Methodology: G.A.Q.-R., C.J.V., D.A.E., M.R.; Formal analysis: G.A.Q.-R., R.J.M., G.L., H.K.V., J.E.H., E.R.P.; Investigation: G.A.Q.-R., R.J.M., G.L., H.K.V., C.J.V., J.E.H., E.R.P.; Resources: D.A.E.; Data curation: G.A.Q.-R., G.L., H.K.V., J.E.H.; Writing - original draft: G.A.Q.-R., J.E.H., E.R.P.; Writing - review & editing: G.A.Q.-R., R.J.M., C.J.V., D.A.E., J.E.H., E.R.P.; Supervision: M.R., J.E.H., E.R.P.; Project administration: J.E.H., E.R.P.; Funding acquisition: J.E.H., E.R.P.

Funding
J.E.H. and E.R.P. acknowledge grant and fellowship support from the National Health and Medical Research Council of Australia, the Heart Foundation of Australia, the Stafford Fox Medical Research Foundation, Stem Cells Australia and QIMR Berghofer Medical Research Institute. The Murdoch Children's Research Institute is supported by the Victorian Government's Operational Infrastructure Support Program.

Data availability
The CHIR hPSC-CM RNA-seq, adult mouse caBCAT RNA-seq and TCF7L2 ChIP-seq datasets have been deposited in GEO under the accession number GSE150521.

Supplementary information
Supplementary information available online at
https://dev.biologists.org/lookup/doi/10.1242/dev.193417.supplemental

Peer review history
The peer review history is available online at
https://dev.biologists.org/lookup/doi/10.1242/dev.193417.reviewer-comments.pdf

References

Alkass, K., Panula, J., Westman, M., Wu, T.-D., Guerquin-Kern, J.-L. and Bergmann, O. (2015). No evidence for cardiomyocyte number expansion in preadolescent mice. *Cell* **163**, 1026-1036. doi:10.1016/j.cell.2015.10.035

Anders, S., Pyl, P. T. and Huber, W. (2015). HTSeq–a Python framework to work with high-throughput sequencing data. *Bioinformatics* **31**, 166-169. doi:10.1093/bioinformatics/btu638

Arany, Z., He, H., Lin, J., Hoyer, K., Handschin, C., Toka, O., Ahmad, F., Matsui, T., Chin, S., Wu, P.-H. et al. (2005). Transcriptional coactivator PGC-1 alpha controls the energy state and contractile function of cardiac muscle. *Cell Metab.* **1**, 259-271. doi:10.1016/j.cmet.2005.03.002

Aurora, A. B., Porrello, E. R., Tan, W., Mahmoud, A. I., Hill, J. A., Bassel-Duby, R., Sadek, H. A. and Olson, E. N. (2014). Macrophages are required for neonatal heart regeneration. *J. Clin. Investig.* **124**, 1382-1392. doi:10.1172/JCI72181

Bassat, E., Mutlak, Y. E., Genzelinakh, A., Shadrin, I. Y., Baruch-Umansky, K., Yifa, O., Kain, D., Rajchman, D., Leach, J., Bassat, D. R. et al. (2017). The extracellular matrix protein Agrin promotes heart regeneration in mice. *Nature* **547**, 179-184. doi:10.1038/nature22978

Bergmann, O., Zdunek, S., Felker, A., Salehpour, M., Alkass, K., Bernard, S., Sjostrom, S. L., Szewczykowska, M., Jackowska, T., dos Remedios, C. et al. (2015). Dynamics of cell generation and turnover in the human heart. *Cell* **161**, 1566-1575. doi:10.1016/j.cell.2015.05.026

Bhalla, K., Liu, W.-J., Thompson, K., Anders, L., Devarakonda, S., Dewi, R., Buckley, S., Hwang, B.-J., Polster, B., Dorsey, S. G. et al. (2014). Cyclin D1 represses gluconeogenesis via inhibition of the transcriptional coactivator PGC1α. *Diabetes* **63**, 3266-3278. doi:10.2337/db13-1283

Bolger, A. M., Lohse, M. and Usadel, B. (2014). Trimmomatic: a flexible trimmer for Illumina sequence data. *Bioinformatics* **30**, 2114-2120. doi:10.1093/bioinformatics/btu170

Bywater, M. J., Burkhart, D. L., Straube, J., Sabò, A., Pendino, V., Hudson, J. E., Quaife-Ryan, G. A., Porrello, E. R., Rae, J., Parton, R. G. et al. (2020). Reactivation of Myc transcription in the mouse heart unlocks its proliferative capacity. *Nat. Commun.* **11**, 1827. doi:10.1038/s41467-020-15552-x

Chen, X., Shevtsov, S. P., Hsich, E., Cui, L., Haq, S., Aronovitz, M., Kerkelä, R., Molkentin, J. D., Liao, R., Salomon, R. N. et al. (2006). The beta-catenin/T-cell factor/lymphocyte enhancer factor signaling pathway is required for normal and stress-induced cardiac hypertrophy. *Mol. Cell. Biol.* **26**, 4462-4473. doi:10.1128/MCB.02157-05

Chen, B., Dodge, M. E., Tang, W., Lu, J., Ma, Z., Fan, C.-W., Wei, S., Hao, W., Kilgore, J., Williams, N. S. et al. (2009). Small molecule-mediated disruption of Wnt-dependent signaling in tissue regeneration and cancer. *Nat. Chem. Biol.* **5**, 100-107. doi:10.1038/nchembio.137

Dobin, A., Davis, C. A., Schlesinger, F., Drenkow, J., Zaleski, C., Jha, S., Batut, P., Chaisson, M. and Gingeras, T. R. (2013). STAR: ultrafast universal RNA-seq aligner. *Bioinformatics* **29**, 15-21. doi:10.1093/bioinformatics/bts635

Duan, J., Gherghe, C., Liu, D., Hamlett, E., Srikantha, L., Rodgers, L., Regan, J. N., Rojas, M., Willis, M., Leask, A. et al. (2012). Wnt1/βcatenin injury response activates the epicardium and cardiac fibroblasts to promote cardiac repair. *EMBO J.* **31**, 429-442. doi:10.1038/emboj.2011.418

Durinck, S., Spellman, P. T., Birney, E. and Huber, W. (2009). Mapping identifiers for the integration of genomic datasets with the R/Bioconductor package biomaRt. *Nat. Protoc.* **4**, 1184-1191. doi:10.1038/nprot.2009.97

D'Uva, G., Aharonov, A., Lauriola, M., Kain, D., Yahalom-Ronen, Y., Carvalho, S., Weisinger, K., Bassat, E., Rajchman, D., Yifa, O. et al. (2015). ERBB2 triggers mammalian heart regeneration by promoting cardiomyocyte dedifferentiation and proliferation. *Nat. Cell Biol.* **17**, 627-638. doi:10.1038/ncb3149

Elliott, D. A., Braam, S. R., Koutsis, K., Ng, E. S., Jenny, R., Lagerqvist, E. L., Biben, C., Hatzistavrou, T., Hirst, C. E., Yu, Q. C. et al. (2011). NKX2-5(eGFP/w) hESCs for isolation of human cardiac progenitors and cardiomyocytes. *Nat. Methods* **8**, 1037-1040. doi:10.1038/nmeth.1740

Eulalio, A., Mano, M., Dal Ferro, M., Zentilin, L., Sinagra, G., Zacchigna, S. and Giacca, M. (2012). Functional screening identifies miRNAs inducing cardiac regeneration. *Nature* **492**, 376-381. doi:10.1038/nature11739

Feng, X.-J., Gao, H., Gao, S., Li, Z., Li, H., Lu, J., Wang, J.-J., Huang, X.-Y., Liu, M., Zou, J. et al. (2015). The orphan receptor NOR1 participates in isoprenaline-induced cardiac hypertrophy by regulating PARP-1. *Br. J. Pharmacol.* **172**, 2852-2863. doi:10.1111/bph.13091

Gilsbach, R., Schwaderer, M., Preissl, S., Grüning, B. A., Kranzhöfer, D., Schneider, P., Nührenberg, T. G., Mulero-Navarro, S., Weichenhan, D., Braun, C. et al. (2018). Distinct epigenetic programs regulate cardiac myocyte development and disease in the human heart in vivo. *Nat. Commun.* **9**, 391. doi:10.1038/s41467-017-02762-z

Gonsalves, F. C., Klein, K., Carson, B. B., Katz, S., Ekas, L. A., Evans, S., Nagourney, R., Cardozo, T., Brown, A. M. C. and DasGupta, R. (2011). An RNAi-based chemical genetic screen identifies three small-molecule inhibitors of the Wnt/wingless signaling pathway. *Proc. Natl. Acad. Sci. USA* **108**, 5954-5963. doi:10.1073/pnas.1017496108

Hahn, J.-Y., Cho, H.-J., Bae, J.-W., Yuk, H.-S., Kim, K.-I., Park, K.-W., Koo, B.-K., Chae, I.-H., Shin, C.-S., Oh, B.-H. et al. (2006). Beta-catenin overexpression reduces myocardial infarct size through differential effects on cardiomyocytes and cardiac fibroblasts. *J. Biol. Chem.* **281**, 30979-30989. doi:10.1074/jbc.M603916200

Heallen, T., Zhang, M., Wang, J., Bonilla-Claudio, M., Klysik, E., Johnson, R. L. and Martin, J. F. (2011). Hippo pathway inhibits Wnt signaling to restrain cardiomyocyte proliferation and heart size. *Science* **332**, 458-461. doi:10.1126/science.1199010

Heinz, S., Benner, C., Spann, N., Bertolino, E., Lin, Y. C., Laslo, P., Cheng, J. X., Murre, C., Singh, H. and Glass, C. K. (2010). Simple combinations of lineage-determining transcription factors prime cis-regulatory elements required for macrophage and B cell identities. *Mol. Cell* **38**, 576-589. doi:10.1016/j.molcel.2010.05.004

Hirose, K., Payumo, A. Y., Cutie, S., Hoang, A., Zhang, H., Guyot, R., Lunn, D., Bigley, R. B., Yu, H., Wang, J. et al. (2019). Evidence for hormonal control of heart regenerative capacity during endothermy acquisition. *Science* **364**, 184-188. doi:10.1126/science.aar2038

Honkoop, H., de Bakker, D. E. M., Aharonov, A., Kruse, F., Shakked, A., Nguyen, P. D., de Heus, C., Garric, L., Muraro, M. J., Shoffner, A. et al. (2019). Single-cell analysis uncovers that metabolic reprogramming by ErbB2 signaling is essential for cardiomyocyte proliferation in the regenerating heart. *eLife* **8**, e50163. doi:10.7554/eLife.50163

Hou, N., Ye, B., Li, X., Margulies, K. B., Xu, H., Wang, X. and Li, F. (2016). Transcription factor 7-like 2 mediates canonical Wnt/β-catenin signaling and c-Myc upregulation in heart failure. *Circ. Heart Failure* **9**, e003010. doi:10.1161/CIRCHEARTFAILURE.116.003010

Huang, D. W., Sherman, B. T., Tan, Q., Collins, J. R., Alvord, W. G., Roayaei, J., Stephens, R., Baseler, M. W., Lane, H. C. and Lempicki, R. A. (2007). The DAVID Gene Functional Classification Tool: a novel biological module-centric algorithm to functionally analyze large gene lists. *Genome Biol.* **8**, R183-R116. doi:10.1186/gb-2007-8-9-r183

Iyer, L. M., Nagarajan, S., Woelfer, M., Schoger, E., Khadjeh, S., Zafiriou, M. P., Kari, V., Herting, J., Pang, S. T., Weber, T. et al. (2018). A context-specific cardiac β-catenin and GATA4 interaction influences TCF7L2 occupancy and remodels chromatin driving disease progression in the adult heart. *Nucleic Acids Res.* **46**, 2850-2867. doi:10.1093/nar/gky049

Langmead, B. and Salzberg, S. L. (2012). Fast gapped-read alignment with Bowtie 2. *Nat. Methods* **9**, 357-359. doi:10.1038/nmeth.1923

Lawrence, M., Huber, W., Pagès, H., Aboyoun, P., Carlson, M., Gentleman, R., Morgan, M. T. and Carey, V. J. (2013). Software for computing and annotating genomic ranges. *PLoS Comput. Biol.* **9**, e1003118. doi:10.1371/journal.pcbi.1003118

Li, Z., Nie, F., Wang, S. and Li, L. (2011). Histone H4 Lys 20 monomethylation by histone methylase SET8 mediates Wnt target gene activation. *Proc. Natl Acad. Sci. USA* **108**, 3116-3123. doi:10.1073/pnas.1009353108

Lin, Z., von Gise, A., Zhou, P., Gu, F., Ma, Q., Jiang, J., Yau, A. L., Buck, J. N., Gouin, K. A., van Gorp, P. R. R. et al. (2014). Cardiac-specific YAP activation improves cardiac function and survival in an experimental murine MI model. *Circ. Res.* **115**, 354-363. doi:10.1161/CIRCRESAHA.115.303632

Magadum, A., Ding, Y., He, L., Kim, T., Vasudevarao, M. D., Long, Q., Yang, K., Wickramasinghe, N., Renikunta, H. V., Dubois, N. et al. (2017). Live cell screening platform identifies PPARδ as a regulator of cardiomyocyte proliferation and cardiac repair. *Cell Res.* **27**, 1002-1019. doi:10.1038/cr.2017.84

Mahmoud, A. I., Kocabas, F., Muralidhar, S. A., Kimura, W., Koura, A. S., Thet, S., Porrello, E. R. and Sadek, H. A. (2013). Meis1 regulates postnatal cardiomyocyte cell cycle arrest. *Nature* **497**, 249-253. doi:10.1038/nature12054

Mahmoud, A. I., O'Meara, C. C., Gemberling, M., Zhao, L., Bryant, D. M., Zheng, R., Gannon, J. B., Cai, L., Choi, W.-Y., Egnaczyk, G. F. et al. (2015). Nerves

regulate cardiomyocyte proliferation and heart regeneration. *Dev. Cell* **34**, 387-399. doi:10.1016/j.devcel.2015.06.017

McLean, C. Y., Bristor, D., Hiller, M., Clarke, S. L., Schaar, B. T., Lowe, C. B., Wenger, A. M. and Bejerano, G. (2010). GREAT improves functional interpretation of cis-regulatory regions. *Nat. Biotechnol.* **28**, 495-501. doi:10.1038/nbt.1630

Mills, R. J., Titmarsh, D. M., Koenig, X., Parker, B. L., Ryall, J. G., Quaife-Ryan, G. A., Voges, H. K., Hodson, M. P., Ferguson, C., Drowley, L. et al. (2017). Functional screening in human cardiac organoids reveals a metabolic mechanism for cardiomyocyte cell cycle arrest. *Proc. Natl Acad. Sci. USA* **114**, E8372-E8381. doi:10.1073/pnas.1707316114

Mills, R. J., Parker, B. L., Quaife-Ryan, G. A., Voges, H. K., Needham, E. J., Bornot, A., Ding, M., Andersson, H., Polla, M., Elliott, D. A. et al. (2019). Drug screening in human PSC-cardiac organoids identifies pro-proliferative compounds acting via the Mevalonate pathway. *Cell Stem Cell* **24**, 895-907.e896. doi:10.1016/j.stem.2019.03.009

Mohamed, T. M. A., Ang, Y.-S., Radzinsky, E., Zhou, P., Huang, Y., Elfenbein, A., Foley, A., Magnitsky, S. and Srivastava, D. (2018). Regulation of cell cycle to stimulate adult cardiomyocyte proliferation and cardiac regeneration. *Cell* **173**, 104-116.e112. doi:10.1016/j.cell.2018.02.014

Nakada, Y., Canseco, D. C., Thet, S. W., Abdisalaam, S., Asaithamby, A., Santos, C. X., Shah, A. M., Zhang, H., Faber, J. E., Kinter, M. T. et al. (2017). Hypoxia induces heart regeneration in adult mice. *Nature* **541**, 222-227. doi:10.1038/nature20173

Natarajan, N., Abbas, Y., Bryant, D. M., González-Rosa, J. M., Sharpe, M., Uygur, A., Cocco-Delgado, L. H., Ho, N. N., Gerard, N. P., Gerard, C. J. et al. (2018). Complement receptor C5aR1 plays an evolutionarily conserved role in successful cardiac regeneration. *Circulation* **137**, 2152-2165. doi:10.1161/CIRCULATIONAHA.117.030801

Noack, C., Zafiriou, M. P., Schaeffer, H. J., Renger, A., Pavlova, E., Dietz, R., Zimmermann, W. H., Bergmann, M. W. and Zelarayán, L. C. (2012). Krueppel-like factor 15 regulates Wnt/beta-catenin transcription and controls cardiac progenitor cell fate in the postnatal heart. *EMBO Mol. Med.* **4**, 992-1007. doi:10.1002/emmm.201101043

Oerlemans, M. I. F. J., Goumans, M.-J., van Middelaar, B., Clevers, H., Doevendans, P. A. and Sluijter, J. P. G. (2010). Active Wnt signaling in response to cardiac injury. *Basic Res. Cardiol.* **105**, 631-641. doi:10.1007/s00395-010-0100-9

Pearen, M. A., Myers, S. A., Raichur, S., Ryall, J. G., Lynch, G. S. and Muscat, G. E. O. (2008). The orphan nuclear receptor, NOR-1, a target of beta-adrenergic signaling, regulates gene expression that controls oxidative metabolism in skeletal muscle. *Endocrinology* **149**, 2853-2865. doi:10.1210/en.2007-1202

Porrello, E. R., Mahmoud, A. I., Simpson, E., Hill, J. A., Richardson, J. A., Olson, E. N. and Sadek, H. A. (2011). Transient regenerative potential of the neonatal mouse heart. *Science* **331**, 1078-1080. doi:10.1126/science.1200708

Porrello, E. R., Mahmoud, A. I., Simpson, E., Johnson, B. A., Grinsfelder, D., Canseco, D., Mammen, P. P., Rothermel, B. A., Olson, E. N. and Sadek, H. A. (2013). Regulation of neonatal and adult mammalian heart regeneration by the miR-15 family. *Proc. Natl Acad. Sci. USA* **110**, 187-192. doi:10.1073/pnas.1208863110

Quaife-Ryan, G. A., Sim, C. B., Porrello, E. R. and Hudson, J. E. (2016). Resetting the epigenome for heart regeneration. *Semin. Cell Dev. Biol.* **58**, 2-13. doi:10.1016/j.semcdb.2015.12.021

Quaife-Ryan, G. A., Sim, C. B., Ziemann, M., Kaspi, A., Rafehi, H., Ramialison, M., El-Osta, A., Hudson, J. E. and Porrello, E. R. (2017). Multicellular transcriptional analysis of mammalian heart regeneration. *Circulation* **136**, 1123-1139. doi:10.1161/CIRCULATIONAHA.117.028252

Ramírez, F., Ryan, D. P., Grüning, B., Bhardwaj, V., Kilpert, F., Richter, A. S., Heyne, S., Dündar, F. and Manke, T. (2016). deepTools2: a next generation web server for deep-sequencing data analysis. *Nucleic Acids Res.* **44**, W160-W165. doi:10.1093/nar/gkw257

Robinson, M. D., McCarthy, D. J. and Smyth, G. K. (2010). edgeR: a Bioconductor package for differential expression analysis of digital gene expression data. *Bioinformatics* **26**, 139-140. doi:10.1093/bioinformatics/btp616

Rumyantsev, P. P. and Borisov, A. (1987). DNA synthesis in myocytes from different myocardial compartments of young rats in norm, after experimental infarction and in vitro. *Biomed. Biochim. Acta* **46**, S610-S615.

Sdek, P., Zhao, P., Wang, Y., Huang, C.-J., Ko, C. Y., Butler, P. C., Weiss, J. N. and MacLellan, W. R. (2011). Rb and p130 control cell cycle gene silencing to maintain the postmitotic phenotype in cardiac myocytes. *J. Cell Biol.* **194**, 407-423. doi:10.1083/jcb.201012049

Soonpaa, M. H., Kim, K. K., Pajak, L., Franklin, M. and Field, L. J. (1996). Cardiomyocyte DNA synthesis and binucleation during murine development. *Am. J. Physiol.* **271**, H2183-H2189. doi:10.1152/ajpheart.1996.271.5.H2183

Taegtmeyer, H., Sen, S. and Vela, D. (2010). Return to the fetal gene program: a suggested metabolic link to gene expression in the heart. *Ann. N. Y. Acad. Sci.* **1188**, 191-198. doi:10.1111/j.1749-6632.2009.05100.x

Tiburcy, M., Hudson, J. E., Balfanz, P., Schlick, S., Meyer, T., Chang Liao, M.-L., Levent, E., Raad, F., Zeidler, S., Wingender, E. et al. (2017). Defined engineered human myocardium with advanced maturation for applications in heart failure modeling and repair. *Circulation* **135**, 1832-1847. doi:10.1161/CIRCULATIONAHA.116.024145

Tward, A. D., Jones, K. D., Yant, S., Cheung, S. T., Fan, S. T., Chen, X., Kay, M. A., Wang, R. and Bishop, J. M. (2007). Distinct pathways of genomic progression to benign and malignant tumors of the liver. *Proc. Natl. Acad. Sci. USA* **104**, 14771-14776. doi:10.1073/pnas.0706578104

Uhlén, M., Fagerberg, L., Hallström, B. M., Lindskog, C., Oksvold, P., Mardinoglu, A., Sivertsson, Å., Kampf, C., Sjöstedt, E., Asplund, A. et al. (2015). Tissue-based map of the human proteome. *Science* **347**, 1260419. doi:10.1126/science.1260419

Voges, H. K., Mills, R. J., Elliott, D. A., Parton, R. G., Porrello, E. R. and Hudson, J. E. (2017). Development of a human cardiac organoid injury model reveals innate regenerative potential. *Development* **144**, 1118-1127. doi:10.1242/dev.143966

von Gise, A., Lin, Z., Schlegelmilch, K., Honor, L. B., Pan, G. M., Buck, J. N., Ma, Q., Ishiwata, T., Zhou, B., Camargo, F. D. et al. (2012). YAP1, the nuclear target of Hippo signaling, stimulates heart growth through cardiomyocyte proliferation but not hypertrophy. *Proc. Natl Acad. Sci. USA* **109**, 2394-2399. doi:10.1073/pnas.1116136109

Wang, S., Ye, L., Li, M., Liu, J., Jiang, C., Hong, H., Zhu, H. and Sun, Y. (2016). GSK-3β inhibitor CHIR-99021 promotes proliferation through upregulating β-catenin in neonatal atrial human cardiomyocytes. *J. Cardiovasc. Pharmacol.* **68**, 425-432. doi:10.1097/FJC.0000000000000429

Wang, W., Hu, C.-K., Zeng, A., Alegre, D., Hu, D., Gotting, K., Ortega Granillo, A., Wang, Y., Robb, S., Schnittker, R. et al. (2020). Changes in regeneration-responsive enhancers shape regenerative capacities in vertebrates. *Science* **369**, eaaz3090. doi:10.1126/science.aaz3090

Wöhrle, S., Wallmen, B. and Hecht, A. (2007). Differential control of Wnt target genes involves epigenetic mechanisms and selective promoter occupancy by T-cell factors. *Mol. Cell. Biol.* **27**, 8164-8177. doi:10.1128/MCB.00555-07

Xin, M., Kim, Y., Sutherland, L. B., Qi, X., McAnally, J., Schwartz, R. J., Richardson, J. A., Bassel-Duby, R. and Olson, E. N. (2011). Regulation of insulin-like growth factor signaling by Yap governs cardiomyocyte proliferation and embryonic heart size. *Sci. Signal.* **4**, ra70. doi:10.1126/scisignal.2002278

Ye, J., Coulouris, G., Zaretskaya, I., Cutcutache, I., Rozen, S. and Madden, T. L. (2012). Primer-BLAST: A tool to design target-specific primers for polymerase chain reaction. *BMC Bioinformatics* **13**, 134. doi:10.1186/1471-2105-13-134

Ye, L., D'Agostino, G., Loo, S. J., Wang, C. X., Su, L. P., Tan, S. H., Tee, G. Z., Pua, C. J., Pena, E. M., Cheng, R. B. et al. (2018). Early regenerative capacity in the porcine heart. *Circulation* **138**, 2798-2808. doi:10.1161/CIRCULATIONAHA.117.031542

Zhang, Y., Liu, T., Meyer, C. A., Eeckhoute, J., Johnson, D. S., Bernstein, B. E., Nussbaum, C., Myers, R. M., Brown, M., Li, W. et al. (2008). Model-based analysis of ChIP-Seq (MACS). *Genome Biol.* **9**, R137. doi:10.1186/gb-2008-9-9-r137

Zhao, X., Hua, Y., Chen, H., Yang, H., Zhang, T., Huang, G., Fan, H., Tan, Z., Huang, X., Liu, B. et al. (2015). Aldehyde dehydrogenase-2 protects against myocardial infarction-related cardiac fibrosis through modulation of the Wnt/β-catenin signaling pathway. *Ther. Clin. Risk Manag.* **11**, 1371-1381. doi:10.2147/TCRM.S88297

Zhou, J., Ahmad, F., Parikh, S., Hoffman, N. E., Rajan, S., Verma, V. K., Song, J., Yuan, A., Shanmughapriya, S., Guo, Y. et al. (2016). Loss of adult cardiac myocyte GSK-3 leads to mitotic catastrophe resulting in fatal dilated cardiomyopathy. *Circ. Res.* **118**, 1208-1222. doi:10.1161/CIRCRESAHA.116.308544

Zhu, W., Zhang, E., Zhao, M., Chong, Z., Fan, C., Tang, Y., Hunter, J. D., Borovjagin, A. V., Walcott, G. P., Chen, J. Y. et al. (2018). Regenerative potential of neonatal porcine hearts. *Circulation* **138**, 2809-2816. doi:10.1161/CIRCULATIONAHA.118.034886